Cardiac overexpression of PDE4B blunts β-adrenergic response and maladaptive remodeling in heart failure

Sarah Karam, Jean Piero Margaria, Aurélia Bourcier, Delphine Mika, Audrey Varin, Ibrahim Bedioune, Marta Lindner, Kaouter Bouadjel, Matthieu Dessillons, Françoise F. Gaudin, et al.

Cardiac overexpression of PDE4B blunts β-adrenergic response and maladaptive remodeling in heart failure

Karam S[1]*, Margaria JP[2]*, Bourcier A[1]*, Mika D[1], Varin A[1], Bedioune I[1], Lindner M[1], Bouadjel K[1], Dessillons M[1], Gaudin F[3], Lefebvre F[1], Mateo P[1], Lechène P[1], Gomez S[1], Domergue V[3], Robert P[3], Coquard C[1], Algalarrondo V[1], Samuel JL[4], Michel JB[5], Charpentier F[6], Ghigo A[2], Hirsch E[2], Fischmeister R[1], Leroy J[1], Vandecasteele, G[1$]

[1]Université Paris-Saclay, Inserm, Signaling and Cardiovascular Pathophysiology, UMR-S 1180, 92296 Châtenay-Malabry, France.

[2]Department of Molecular Biotechnology and Health Sciences, Molecular Biotechnology Center, University di Torino, 10126 Torino, Italy.

[3]Université Paris-Saclay, Inserm, UMS-IPSIT, 92296 Châtenay-Malabry, France.

[4]UMR-S 942, INSERM, Paris University, 75010 Paris, France.

[5]UMR-S 1148, INSERM, Paris University, X. Bichat hospital, 75018 Paris, France.

[6]Institut du thorax, INSERM, CNRS, Univ. Nantes, 8 quai Moncousu, 44007 Nantes cedex 1, France.

Running title: *Augmenting PDE4B limits heart failure*

*Equal contribution.

[$]To whom correspondence should be addressed:

Grégoire Vandecasteele, PhD
Laboratory of Signaling and Cardiovascular Pathophysiology, INSERM UMR-S 1180
Faculty of Pharmacy
5, rue JB Clément
92296 Châtenay-Malabry
France
Tel: +33 1 46 83 57 17
Fax: +33 1 46 83 54 75
E-mail: gregoire.vandecasteele@universite-paris-saclay.fr

ABSTRACT

Background The cAMP-hydrolyzing phosphodiesterase 4B (PDE4B) is a key negative regulator of cardiac β-adrenergic (β-AR) stimulation. PDE4B deficiency leads to abnormal Ca^{2+} handling and PDE4B is decreased in pressure overload hypertrophy, suggesting that increasing PDE4B in the heart is beneficial in heart failure (HF).

Methods: We measured PDE4B expression in human cardiac tissues, developed two transgenic mouse lines with cardiomyocyte-specific overexpression of PDE4B (PDE4B-TG), and an adeno-associated virus serotype 9 encoding PDE4B (AAV9-PDE4B). Myocardial structure and function were evaluated by echocardiography, ECG, and in Langendorff-perfused hearts. Cyclic AMP and PKA activity were monitored by Förster resonance energy transfer, $I_{Ca,L}$ by whole cell patch-clamp, and cardiomyocyte shortening and Ca^{2+} transients with an Ionoptix® system. HF was induced by 2 weeks infusion of isoproterenol (Iso) or transverse aortic constriction (TAC). Cardiac remodeling was evaluated by serial echocardiography, morphometric analysis and histology.

Results: PDE4B protein was decreased in human failing hearts. The first PDE4B-TG mouse line (TG15) had a ~15-fold increase in cardiac cAMP-PDE activity and a ~30% decrease in cAMP content and fractional shortening associated with a mild cardiac hypertrophy that resorbed with age. Basal *ex vivo* myocardial function was unchanged, but β-AR stimulation of cardiac inotropy, cAMP, PKA, $I_{Ca,L}$, Ca^{2+} transients and cell contraction were blunted. Endurance capacity and life expectancy were normal. Moreover, these mice were protected from systolic dysfunction, hypertrophy, lung congestion and fibrosis induced by chronic Iso treatment. In the second transgenic mouse line (TG50), markedly higher PDE4B overexpression, resulting in a ~50-fold increase in cardiac cAMP-PDE activity caused a ~50% decrease in fractional shortening, hypertrophy, dilatation and premature death. In contrast, mice injected with AAV9-PDE4B (10^{12} viral particles/mouse) had a ~50% increase in cardiac cAMP-PDE activity which did not modify basal cardiac function but efficiently prevented systolic dysfunction, apoptosis and fibrosis, while attenuating hypertrophy induced by chronic Iso

infusion. Similarly, AAV9-PDE4B slowed contractile deterioration, attenuated hypertrophy and lung congestion and prevented apoptosis and fibrotic remodeling in TAC.

Conclusions: Our results indicate that a moderate increase in PDE4B is cardioprotective and suggest that cardiac gene therapy with PDE4B might constitute a new promising approach to treat HF.

What is new ?

- The cAMP-hydrolyzing enzyme PDE4B is decreased in human failing hearts.
- Cardiac overexpression of PDE4B in mice resulting in a 15-fold increase in cAMP hydrolysis decreases cardiac contraction and protects against the cardiotoxic effects of chronic β-adrenergic stimulation, whereas transgenic mice with a 50-fold increase in cardiac cAMP hydrolysis undergo maladaptive remodeling.
- Cardiac PDE4B gene transfer with serotype 9 adeno-associated viruses (AAV9) resulting in a significantly lower increase in cardiac PDE4B protects against chronic catecholamine stimulation and trans-aortic constriction, without depressing basal cardiac function.

What are the clinical implications ?

- Our results suggest that a moderate increase in cardiac PDE4B is beneficial to counteract the detrimental effect of excessive sympathetic system activation in heart failure.
- An increase in PDE4B in the human heart could be achieved by gene therapy with AAV9 or by using recently developed small molecules with PDE4-activating properties.

INTRODUCTION

Heart failure (HF) is the final common stage of many cardiovascular disorders including myocardial infarction and hypertension as common causes. Regardless of the underlying cause for HF, patients show a hyper-active sympathetic nervous system with elevated plasma catecholamine levels that correlate with disease severity.[1] Although beneficial on the short term, prolonged sympathetic stimulation promotes cardiac hypertrophy, myocardial cell death, fibrosis, and arrhythmias.[2] Accordingly, β-blockers improve survival in patients with chronic low ejection fraction[3] and are a mainstay of current HF therapy. However, in most instances, β-blockers can only slow disease progression and may cause significant side effects in some patients. Thus, there is a need for improved therapeutics in HF, alternative or complementary to β-blockers.

The β-adrenergic stimulation of cardiac function involves the second messenger cAMP which activates the cAMP-dependent protein kinase (PKA) to modulate key proteins of the excitation-contraction coupling (ECC) process. These include sarcolemmal L-type Ca^{2+} channels (LTCC) that underlie the L-type Ca^{2+} current ($I_{Ca,L}$), ryanodine receptors (RyR2), phospholamban (PLB), troponin I and myosin-binding protein C.[4] The intracellular levels of cAMP are determined by the balance between synthesis by adenylyl cyclases and degradation by cyclic nucleotide phosphodiesterases (PDEs). PDEs represent a highly diverse superfamily of enzymes, regrouped into 11 families according to their primary structure, enzymatic properties, regulation and pharmacology.[5] Among these, PDE3 and PDE4 are the main PDEs degrading cAMP with a high affinity in the heart and are critical to control the termination of cardiac β-AR responses.[6] Inhibition of PDE4 results in a massive potentiation of cAMP during β-AR stimulation not only in rodent[6] but also in dog,[7] pig[8] and human cardiomyocytes.[9] As a consequence, PDE4 activity modulates β-AR stimulation of $I_{Ca,L}$ and ECC in these species.[6, 9, 10] PDE4 inhibition also increases cellular hypertrophy[11] and sarcoplasmic reticulum (SR) Ca^{2+} leak, thereby favoring cardiac arrhythmias.[10]

The PDE4 family is encoded by four genes (*Pde4a-Pde4d*), but only three (*Pde4a*, *Pde4b*, and *Pde4d*) are expressed in the human and rodent heart.[12] Whereas PDE4D was proposed to associate with RyR2 to control SR Ca^{2+} release[13] and with PLB to control SR Ca^{2+} reuptake[14] we have found that PDE4B is physically associated to the principal $Ca_V1.2$ subunit of LTCCs to modulate β-AR regulation of $I_{Ca,L}$.[15] *Pde4d* knock-out mice have enhanced SR Ca^{2+} leak and arrhythmias and develop HF with age,[13] whereas *Pde4b* knock-out mice have exaggerated β-AR stimulation of $I_{Ca,L}$ and Ca^{2+} transients, leading to increased spontaneous Ca^{2+} waves and enhanced susceptibility to ventricular tachycardia.[15] PDE4B expression and activity are decreased in a rat model of pathological hypertrophy induced by pressure overload,[16] suggesting that increasing PDE4B in the heart could be beneficial in HF. To test this hypothesis, we first measured PDE4B expression in human hearts and found that it was decreased in HF. We then generated transgenic mice with cardiac-specific overexpression of PDE4B, and found that constitutive cardiac PDE4B overexpression decreases cardiac contractile function, blunts β-AR responses, and protects against the detrimental effects of chronic isoproterenol (Iso) infusion. To further examine the therapeutic potential of PDE4B, the gene was delivered to the heart with adeno-associated virus 9 (AAV9). This approach resulted in a drastic improvement of cardiac function in the chronic Iso model, and significantly delayed contractile dysfunction and attenuated remodeling induced by transverse aortic constriction (TAC) without impacting normal cardiac function. These results suggest that increasing PDE4B with gene therapy could represent a novel therapeutic strategy to treat HF.

METHODS

An expanded methods section is available in the Data supplement.

The authors declare that all supporting data are available within the article and its online supplementary files. Human heart tissue was obtained from the cardiovascular biobank of Bichat

Hospital (BB-0033-00029, coordinator Dr. JB Michel) and from a tissue collection from the Pitié-Salpétrière Hospital (coordinator Dr. JL Samuel), with approval by the Inserm Institutional Review Board and the Consultative Committee for the Protection of Human Subjects in Biomedical Research at the Pitié-Salpétrière Hospital, respectively. Patients or their relatives were informed that anonymized tissue will be used for research and given the right to refuse. All experiments involving animals were carried out according to the European Community guiding principles in the care and use of animals (2010/63/UE), the local Ethics Committee (CREEA Ile-de-France Sud) guidelines and the French decree n° 2013-118 on the protection of animals used for scientific purposes. Mice overexpressing the murine PDE4B3 (NCBI NM_019840.2) under the α-MHC promoter (PDE4B-TG mice) were generated by pronuclear injection and the genotype was confirmed by PCR. Male PDE4B-TG mice and age-matched WT littermates were used for experiments. AAV9 encoding the murine PDE4B3 (NCBI NM_019840.2) or luciferase under the control of a CMV promoter were produced in AAV-293T cells. PDE4B3 expression as well as hypertrophic and fibrosis markers were evaluated by qRT-PCR. PDE expression was assessed by western blot, PDE activity by radioimmunoassay, and cAMP by ELISA. Transthoracic two-dimensional-guided M-mode echocardiography was performed with a ML6 linear probe of 15 MHz under 2% isoflurane gas and 0.8 L/min oxygen anaesthesia. Six-lead surface electrocardiograms (ECG) were recorded during isoflurane inhalation and telemetric ECG transmitters were used to record ECG in freely roaming animals. *Ex vivo* cardiac function was evaluated in Langendorff heart preparations. Isolated cardiomyocyte studies: β-AR regulation of cAMP levels and PKA activity were assessed by optical FRET methods. $I_{Ca,L}$ was recorded with the patch-clamp technique, sarcomere shortening and Ca^{2+} transients with an Ionoptix® system. Pathological cardiac remodeling was induced by chronic Iso infusion (60 mg/kg/day during 14 days) using osmotic minipumps or by TAC.

RESULTS

PDE4B expression is decreased in human heart failure

To determine whether PDE4B is decreased in human HF like in experimental pathological hypertrophy,[16] PDE4B protein was measured by western blot in human heart samples collected from two Parisian hospitals. As shown in Figure 1, PDE4B protein expression was significantly decreased in hearts with either ischemic (Figure 1A) or dilated cardiomyopathy compared to non-failing controls (Figure 1B).

Cardiac phenotype of PDE4B transgenic mice

To evaluate the role of PDE4B in controlling cardiac function, two transgenic mouse lines with cardiomyocyte-specific overexpression of PDE4B3, the main PDE4B isoform expressed in the mouse myocardium,[17] were generated (PDE4B-TG). In the first line, PDE4B mRNA and protein were increased ~50-fold compared to wild-type (WT), resulting in a ~25-fold increase in PDE4 activity and ~15-fold increase in total cardiac cAMP-hydrolytic activity (Fig. 2A-D). Hence, in the following this line is referred to as TG15. Consistent with increased PDE activity, cAMP was significantly decreased by ~30% in hearts from these mice (Fig. 2E). The expression of other major PDEs hydrolyzing cAMP in the heart (PDE3A, PDE4A and PDE4D) was not modified in TG15 mice compared to WT (Supplemental Fig. 1).

To evaluate the consequences of PDE4B overexpression on cardiac structure and function, young WT and TG15 male mice (10-15 weeks) were subjected to echocardiography and anatomical analysis. Cardiac contractility, quantified as fractional shortening (FS), was significantly decreased by ~30% in TG15 mice (Fig. 2F). This result is in line with the reduced cAMP content, and suggests that PDE4B overexpression counteracts the positive inotropic effect of the endogenous sympathetic stimulation. In contrast, heart rate was unchanged (Fig. 2F). Echocardiography also revealed a trend toward an increase in left ventricle weight (Fig. 2F), a result that was confirmed by morphometric analysis (Fig. 2G), which indicated a mild but significant cardiac hypertrophy in TG15 mice, whereas

lung weight was unchanged (Fig. 2G and Supplemental Table 1). Along with decreased FS, the phosphorylation of phospholamban (PLB), troponin I (TnI) and myosin-binding protein C (MyBPC) at PKA sites was decreased in cardiac tissues from TG15 mice (Fig 2H-J). In addition, PLB phosphorylation at Threonine 17, a specific CaMKII site, was also decreased (Fig. 2H).

In the course of this study, we characterized a second line of PDE4B-TG mice with substantially higher levels of overexpression: PDE4B mRNA was increased ~900-fold and total cAMP-hydrolytic activity was increased ~50-fold (Supplemental Fig. 2A, B). Hence this line is referred to as TG50 in the rest of the study. FS was decreased by ~50% in TG50, and this was accompanied by increased left ventricle (LV) dimension and mass, although there was no sign of pulmonary congestion (Supplemental Fig. 2C, D). Heart rate (HR) measured by echocardiography tended to be decreased in TG50, although the difference was not statistically significant (Supplemental Fig. 2C). In order to exclude confounding effects of anesthesia, telemetric ECG recordings were performed in freely roaming WT, TG15 and TG50 mice across a circadian cycle (Supplemental Fig. 3A). These measurements confirmed that HR was unchanged in TG15, whereas in TG50, HR was decreased during daytime, both at rest and during exercise on a treadmill (Supplemental Fig. 3A and 3B). To determine whether this bradycardia was related to a difference in transgene expression at the supraventricular level, PDE4B protein was measured in the left ventricle, left atria and dissected sino-atrial node (SAN) of WT, TG15 and TG50. As shown in Supplemental Fig. 3C, PDE4B was modestly increased in SAN from TG15 whereas it was strongly overexpressed in TG50. Intriguingly, exercise capacity, as determined by the maximal distance run on a treadmill until exhaustion, was not different between WT and PDE4B-TG mice, with even a trend for increased distance run in TG15 compared to WT mice (Supplemental Fig. 3D).

To assess the long term consequences of cardiac PDE4B overexpression, serial echocardiography was performed in both lines during aging. As shown in Fig. 3A and 3B, in TG50 there was a progressive deterioration of systolic function accompanied by a prominent cardiac hypertrophy and

dilatation. This led to premature death, with 50% mortality at 72 weeks (Fig. 3C). In contrast, in TG15, although FS remained lower than in WT, cardiac hypertrophy actually normalized with aging, and mortality was similar to WT (Fig. 3A-C). Consistent with these results, the fetal marker genes *Nppa*, *Nppb* and *Myh7* were strongly re-expressed in hearts from TG50, both in young (10-15 weeks) and old (58-60 weeks) mice, whereas in TG15 these genes tended to be increased in young but normalized in old (Supplemental Fig. 4A-C). This pattern was also observed for *Rcan1*, a specific target gene of the calcineurin-NFAT pathway.[18] These results show that while substantial PDE4B overexpression in TG15 is well tolerated, drastic cardiac PDE4B overexpression in TG50 is detrimental. The reversible hypertrophy in TG15 suggested a potential role of PDE4B in physiological hypertrophy. Physiological hypertrophy has been associated with activation of the RAC-alpha serine/threonine-protein kinase (AKT), which can directly phosphorylate and inhibit glycogen synthase kinase 3β (GSK3β), and with activation of ERK1/2.[19] However, the phosphorylation of these kinases was similar between young WT and TG15 (Supplemental Figure 5). In contrast, the phosphorylation AKT and GSK3β were decreased in TG50 compared to WT mice, whereas that of ERK1/2 was increased. While these results do not support the implication of these pathways in the reversible hypertrophy of TG15, they suggest their contribution to the development of maladaptive remodeling in TG50. In the following, we focused on the detailed phenotypic characterization of the TG15 mouse line.

PDE4B overexpression blunts β-AR stimulation of heart function

To determine the role of PDE4B under acute β-AR stimulation, we first evaluated cardiac function under Iso infusion in anesthetized mice by echocardiography and ECG. As shown in Fig. 4A and 4B, Iso increased FS and heart rate, which were significantly lower in TG15 than in WT hearts. To better assess the intrinsic properties of TG15 mouse hearts, isolated Langendorff-perfused hearts were investigated (Fig 4C-F). The developed pressure was similar in WT and TG15 hearts, revealing preserved contractile capacities of TG hearts in basal conditions (Fig. 4C). Basal heart rate was also

unaffected by PDE4B overexpression (Fig. 4D), in agreement with the *in vivo* data. To evaluate β-adrenergic responsiveness, increasing concentrations of Iso were applied in hearts paced at 650 bpm(Fig. 4E). Hill fit of the data revealed a significantly increased EC_{50} value for Iso in TG15 hearts compared to WT (Fig. 4F). Similar results were observed on the maximal rates of contraction and relaxation (Supplemental Fig. 6).

PDE4B overexpression blunts β-AR responses in isolated cardiomyocytes

To investigate how PDE4B overexpression affects the β-AR signaling cascade, intracellular cAMP and PKA activity were monitored in isolated ventricular myocytes expressing the FRET biosensors EPAC-S^{H187} [20] and AKAR3-NES[21], respectively. Whereas a brief application of Iso (30 nmol/L, 15s) produced a robust cAMP elevation in WT cells (+177% increase of the FRET ratio), it increased the FRET ratio by only ~35% in TG15 cells (Supplemental Fig. 7A). Similarly, PKA activation was strongly blunted (~15% increase in FRET ratio) in TG15 *versus* WT cardiomyocytes (~53% increase in FRET ratio, Supplemental Fig. 7B). As a consequence, the β-AR stimulation of $I_{Ca,L}$ was severely diminished in TG15 myocytes (Supplemental Fig. 7C), while basal $I_{Ca,L}$ density remained unchanged (WT: 7.0±0.3 pA/pF, n=44; TG:7.4±0.2 pA/pF, n=84). Importantly, attenuated β-AR responses in TG15 myocytes were restored to WT levels in the presence of the selective PDE4 inhibitor, Ro 20-1724 (Supplemental Fig. 8A-C). Next, we measured Ca^{2+} transient and sarcomere shortening amplitudes in isolated ventricular myocytes (Fig. 5A-E), which revealed an attenuation of the inotropic and lusitropic effects of β-AR stimulation, whereas basal values were similar between WT and TG15 mice. Again, these effects were normalized by PDE4 inhibition (Supplemental Fig. 8D, E). These results are in line with the preserved basal cardiac function and the diminished β-AR responsiveness observed *ex vivo*. Furthermore, whereas about 80% of isolated WT ventricular myocytes exposed to Iso showed frequent occurrences of spontaneous Ca^{2+} release events (SCRs), SCRs were rare in cardiomyocytes isolated from TG15 mice, and occurred in less than 50% of the

cells (Fig. 5G, H). Thus, PDE4B overexpression protects against proarrhythmogenic events triggered by β-AR stimulation.

PDE4B overexpression protects from maladaptive remodeling induced by chronic infusion of isoproterenol

To determine the potential protective effects of cardiac PDE4B overexpression under stress conditions, WT and TG15 mice were subjected to chronic Iso infusion. Cardiac function was evaluated by echocardiography on the day of osmotic minipump implantation, at the end of the 2 weeks treatment, and before sacrifice at 4 weeks (Fig. 6A). WT and TG15 mice implanted with Iso minipumps displayed an increase in heart rate at two weeks, attesting the adequate infusion of the drug (Supplemental Fig. 9A). Interestingly, chronic Iso infusion decreased FS at 2 and 4 weeks in WT mice, while it was first increased then preserved in TG15 (Fig. 6B). Chronic Iso also significantly increased LV mass in WT but not in TG15 mice (Fig. 6B), a finding that was corroborated by measurements of heart weight to tibia length ratio at the time of sacrifice (Fig. 6C). Moreover, Iso increased lung weight in WT but not in TG15 mice (Fig. 6C). Finally, whereas Iso induced cardiac fibrosis in the LV of WT mice, it was drastically reduced in TG15 mice (Fig. 6D). Thus, these results indicate that despite their reduced basal contractile function, TG15 mice were protected against the maladaptive remodeling induced by chronic catecholamine infusion.

To further examine the therapeutic potential of enhanced cardiac PDE4B activity, adeno-associated type 9 viruses (AAV9) were engineered to express this isoform, while a virus encoding luciferase (Luc) was used as control (Supplemental Fig. 10A). We first conducted a pilot study on a limited number of healthy mice to validate our procedure. In these preliminary experiments, tail vein injection of 10^{12} AAV9-PDE4B viral particles led to a ~2-fold increase of PDE4B protein in the heart and a ~50% increase in total cardiac cAMP-hydrolytic activity 8 weeks after injection (Supplemental Fig. 10B and 10C). Interestingly, in contrast to what we observed in PDE4B-TG mice, this mild

overexpression of PDE4B did not decrease FS (Supplemental Fig. 10D) nor did it induce cardiac hypertrophy or lung congestion (Supplemental Fig. 10E, F). We then tested whether PDE4B gene therapy could prevent HF induced by chronic Iso stimulation. For this, mice were injected with 10^{12} viral particles of either AAV9-Luc or AAV9-PDE4B two weeks before minipump implantation and were followed by serial echocardiography during 6 weeks (Fig. 7A). As shown in Fig. 7B, the decrease in FS induced by chronic Iso in control mice expressing Luc was virtually absent in animals expressing PDE4B. In addition, PDE4B overexpression partially prevented LV hypertrophy induced by chronic Iso (Fig. 7B). Although PDE4B gene therapy could not fully prevent the increase in heart weight induced by Iso (Fig. 7C), Iso-induced fibrosis and apoptosis were prevented by AAV9-mediated PDE4B overexpression (Fig. 7D, E). Western blot analysis indicated that myocardial PDE4B protein was increased ~5-fold in AAV9-PDE4B injected mice (Supplemental Fig. 11A). In summary, AAV9-mediated cardiac PDE4B overexpression partially prevented hypertrophy, but importantly, preserved against the cardiac dysfunction and remodeling induced by chronic Iso stimulation.

Next, cardiac gene therapy with PDE4B was evaluated in mice with transverse aortic constriction (TAC). Two days after the surgery, mice with a pressure gradient across the aorta ≥60 mmHg were randomly injected with either AAV9-Luc or AAV9-PDE4B (10^{12} viral particles/mouse) and followed by serial echocardiography during six weeks (Fig. 8A). Although the extent of depressed FS was ultimately similar in mice injected with PDE4B compared to Luc, this decrease was significantly less pronounced at day 14, indicating that PDE4B overexpression delayed cardiac contractile dysfunction induced by TAC (Fig. 8B). In addition, PDE4B overexpression attenuated cardiac hypertrophy and pulmonary congestion induced by TAC (Fig. 8B, C) and reduced both fibrosis and apoptosis (Fig. 8D, E). Similar to what we observed in mice treated with Iso, cardiac PDE4B protein was increased ~6-fold in TAC mice injected with AAV9-PDE4B (Supplemental Fig. 11B).

DISCUSSION

In the present study, we tested whether the cAMP-specific PDE4B is decreased in human HF as reported previously in pressure overload-induced hypertrophy in rats.[16] We characterized the phenotype of mice with myocardial overexpression of PDE4B and we tested whether increasing cardiac PDE4B confers protection against catecholamine toxicity and HF induced by pressure overload. Our main findings can be summarized as follows. First, PDE4B is decreased in failing human hearts compared to non-failing controls. Second, constitutive cardiac PDE4B overexpression in mice counteracts β-adrenergic stimulation of contractile function, which is well tolerated along life span in mice with a ~15-fold increase in cardiac cAMP-PDE activity (TG15), but becomes detrimental at higher levels (~50-fold increase in cardiac cAMP-PDE activity, TG50). Third, TG15 mice are protected from the pathological remodeling elicited by chronic β-adrenergic stimulation, including cardiac hypertrophy, systolic dysfunction, and fibrosis development. Fourth, cardiac PDE4B gene transfer with AAV9, resulting in a significantly lower increase in PDE4B protein and cAMP-PDE activity, also protected against chronic catecholamine stimulation and trans-aortic constriction, without depressing basal cardiac function. These results suggest that decreased PDE4B is maladaptive in HF and that a moderate PDE4B activation in the heart achieved by AAV9-mediated gene transfer could constitute a new promising strategy to limit the systolic dysfunction and pathological remodeling in HF.

Although PDE4 is known to be conserved in rodent, pig and human myocardium[8, 12] there is little information about its expression in human HF and, to our knowledge, nothing concerning PDE4B. Our present results show that this variant is expressed in non-failing human hearts, and is decreased in HF. This finding, together with studies reporting decreased PDE4A and PDE4D in human failing hearts[12, 13] indicates that the three PDE4 isoforms expressed in heart are reduced in human HF, a result

that may explain in part the reported lack of effect of PDE4 inhibitors on force in the failing human myocardium.[22, 23]

TG15 mice had a decreased contractility but preserved heart rate, whereas in TG50 contractility was further depressed and this was associated with bradycardia. Our results in Supplemental Fig. 3 show that these differences are the consequence of a higher expression of PDE4B in TG50, both in the ventricles and in the SAN. Lower expression of the transgene in TG15 SAN *versus* ventricle may be explained by a position effect secondary to random insertion of the transgene.[24] The less obvious effect of PDE4B overexpression on heart rate *versus* contractility may also be related to the mouse model. Indeed, previous studies found little chronotropic response to PDE4 inhibition in mice[25] compared to rats.[26] In TG15, PDE4B overexpression was associated with decreased cAMP content and depressed phosphorylation of the major proteins involved in ECC. In addition, β-AR stimulation of cAMP production, PKA, $I_{Ca,L}$, Ca^{2+} transients and cell contraction, as well as of developed pressure in isolated hearts, were attenuated in TG15. The reason why the maximal effect of Iso on developed pressure was similar in isolated perfused hearts from TG15 and WT mice (Fig. 4C) whereas maximal sarcomere shortening was decreased in TG15 myocytes (Fig. 5B) remains unclear. Nevertheless, these results are consistent with the key role of PDE4 in modulating β-AR responses in the rodent heart.[6, 27] The decreased β-AR stimulation of $I_{Ca,L}$ and of pro-arrhythmic Ca^{2+} release events in TG15 mice confirms the importance of PDE4B for LTCC regulation, as previously inferred from studies in PDE4 knock-out mice[15], while the decreased PLB, TnI and MyBPC phosphorylation indicates that in TG15, the overexpressed PDE4B also impacts other critical proteins for ECC.

The phenotype of TG15 mice reported here is, in several aspects, similar to that of mice with a ~10-fold overexpression of PDE3A in the heart.[28] This may not be too surprising, given that PDE3A represents the other major cAMP-PDE regulating cardiac function. One notable difference however, was that PDE3A-TG mice showed bradycardia, whereas heart rate was unchanged in TG15 mice. Although not determined in the study of Oikawa *et al.*[28], this difference might be due to a high

expression of the transgene in the SAN in PDE3A-TG mice. Alternatively, it could be due to different enzymatic properties or localization of these two PDEs. However, upon Iso challenge, heart rate was significantly lower in TG15 mice (Fig. 4), suggesting that PDE4B may contribute to SAN function during sympathetic stimulation. This could be due to the propensity of long PDE4 isoforms—including the PDE4B3 variant overexpressed here—to be phosphorylated and activated by PKA upon β-AR stimulation.[6, 29] Whereas the phenotype of PDE4B-TG mice resembles that of PDE3A-TG mice, it is nearly opposite to that of PDE2-TG mice in which bradycardia is associated with an increase in contractile force presumably due to increased diastolic filling.[30] Although the exact reason for such difference remains uncertain, the lower affinity of PDE2 for cAMP should make this PDE more efficient to degrade the high cAMP levels present in the SAN compared to the ventricles.[31]

The intracellular blockade of β-AR stimulation by PDE4B induced adaptive changes of the heart, but was devoid of overt pathological consequences in TG15. Indeed, basal contractile parameters were similar in isolated hearts from WT and TG15 mice, indicating that constitutive PDE4B overexpression is not detrimental *per se*. Moreover, PDE4B overexpression did not negatively impact on maximal exercise capacity and there was even a tendency for increased distance run in TG15 mice. Although counterintuitive at first sight, it should be noted that Iso was still able to enhance cardiac performance in TG15 mice (Fig. 4), indicating the persistence of a significant cardiac reserve. A similar phenotype was observed in β_1-AR and double β_1-/β_2-AR knock-out mice, despite a near total impediment of chronotropic and inotropic reserve,[32, 33] suggesting the contribution of intrinsic preload and afterload mechanisms in the adaptive response to exercise. It should also be acknowledged that the maximum running distance until exhaustion depends on a number of other factors, among which skeletal muscle capacity is critical.[34] This is certainly one reason for the difference observed with β-blockers in healthy subjects, especially the non-selective ones, which affect endurance capacity not only by their direct effects on the heart, but also by impacting skeletal muscle adaptation and metabolism as well as vascular and lung functions.[35]

The mild cardiac hypertrophy observed in young TG15 mice was associated with transient induction of the brain natriuretic peptide gene *Nppb* and the calcineurin/NFAT target gene *Rcan1*. In contrast, AKT and ERK1/2, which have been associated with adaptive hypertrophy,[19] were not activated in young TG15 mice. These results differ with those obtained in TG50 mice, in which persistent expression of fetal genes and *Rcan1* was associated with progressive cardiac hypertrophy, dilatation, and HF. These results are consistent with the notion that transient calcineurin/NFAT activation can contribute to physiological hypertrophy induced by exercise[36] or pregnancy[37] whereas permanent and excessive activation promotes pathological hypertrophy and HF.[38] Unexpectedly, ERK1/2 was activated in young TG50, suggesting that it contributes to the hypertrophic response, as it does in early stages of pathological hypertrophy induced by TAC.[39] Importantly, AKT and GSK3β phosphorylation were decreased in TG50. Given the well described cardioprotective effects of AKT,[40] decreased activation of this kinase appears as an important contributor to maladaptive remodeling in TG50. Indeed, these results are consistent with increased maladaptive hypertrophy observed in *Akt1*-knockout mice[41] and with studies showing that in the context of pressure overload, decreased phosphorylation of AKT and of GSK3β are associated with cardiac dilatation and the transition to HF.[42, 43]

Importantly, our results show that TG15 mice were protected against pathological cardiac remodeling induced by chronic Iso infusion, although these results were mitigated by the reduced contractile function. However, cardiac delivery of PDE4B using an AAV9 resulted in a significantly lower increase in myocardial PDE4B protein which did not modify cardiac function in healthy mice, but efficiently protected against the detrimental effects of chronic Iso treatment and TAC. Indeed, in both models AAV9-mediated PDE4B overexpression counteracted the systolic dysfunction, attenuated the hypertrophic response, and efficiently prevented fibrosis, a hallmark of pathological remodeling. Replacement interstitial fibrosis as observed here is a known consequence of cardiomyocyte death which occurs in both chronic Iso infusion models[44] and TAC models.[45] Accordingly, our results show

that apoptosis induced by chronic Iso and TAC was prevented in mice treated with AAV9-PDE4B. Several studies have demonstrated that Ca^{2+} overload triggered by PKA-mediated β-AR stimulation of $I_{Ca,L}$ is a critical mechanism for cardiomyocyte death and HF development.[46, 47] Thus, our present finding that PDE4B overexpression blunts β-AR stimulation of PKA activity and $I_{Ca,L,}$ provides a likely explanation for the potent anti-fibrotic action of PDE4B overexpression. This does not exclude that PDE4B acts on other determinants of cardiomyocyte death. For instance, PDE4B decreased CaMKII-mediated PLB phosphorylation (Fig 2H), which was proposed to be involved in CaMKII-mediated apoptosis *in vivo.*[48]

In conclusion, our study demonstrates the potential benefits of increasing PDE4B to limit the cardiotoxic effects of chronic sympathetic stimulation and HF development in mice. Our results also underline the critical importance of transgene dosage for the beneficial or detrimental outcome of cardiac gene manipulation, as previously noted in the case of the β_2-ARs.[49] In this regard, the moderate increase in PDE4B conferred by AAV9 injection appears sufficient to counteract the adverse remodeling induced by chronic Iso and TAC while minimally impacting on normal cardiac function. One limit of our study is the low clinical applicability of these models, hence future studies should be performed in more relevant models such as myocardial infarction. Interestingly, long PDE4 isoforms such as PDE4B3 possess a PKA consensus phosphorylation site in Upstream Conserved Region 1 (UCR1) which, when phosphorylated, activates the enzyme.[17] Recently, a small allosteric modulator that mimics the effect of PKA phosphorylation on PDE4 long forms was reported.[50] This prototypical PDE4 activator was shown to reduce the chronically elevated cAMP levels which drive abnormal cyst formation in animal and human cell models of autosomal dominant polycystic kidney disease.[50] These results suggest that such compound could constitute an alternative approach to gene therapy in HF.

ACKNOWLEDGEMENTS

We thank Agnès Hivonnait (Institut du thorax) for help with ECG recordings and Dr. Kees Jalink (The Netherlands Cancer Institute) for the Epac-S^{H187} sensor.

SOURCES OF FUNDING

UMR-S1180 is a member of the Laboratory of Excellence LERMIT supported by the French National Research Agency (ANR-10-LABX-33) under the program "Investissements d'Avenir" ANR-11-IDEX-0003-01. This work was also funded by grant ANR-19-CE14-0038-02 to GV, ANR-16-ECVD-0007-01 to RF, ANR-16-CE14-0014 to DM, a grant from the Fédération Française de Cardiologie to VA, and grants from Italian Ministry of Health (RF-2013-02354892) and Fondazione Cariplo (2015-0880) to AG. SK was supported by Fondation Lefoulon-Delalande, JPM by the VINCI program of Università Italo-Francese (UIF-UFI), MD, KB and ML by the French Ministère de l'Enseignement Supérieur, de la Recherche et de l'Innovation, IB and DM by the CORDIMM program of Région Ile-de-France and Fondation pour la Recherche Médicale.

DISCLOSURES

None.

REFERENCES

1. Cohn JN, Levine TB, Olivari MT, Garberg V, Lura D, Francis GS, Simon AB and Rector T. Plasma norepinephrine as a guide to prognosis in patients with chronic congestive heart failure. *N Engl J Med*. 1984;311:819-23.

2. El-Armouche A and Eschenhagen T. Beta-adrenergic stimulation and myocardial function in the failing heart. *Heart Fail Rev*. 2009;14:225-41.

3. Effect of metoprolol CR/XL in chronic heart failure: Metoprolol CR/XL Randomised Intervention Trial in Congestive Heart Failure (MERIT-HF). *Lancet*. 1999;353:2001-7.

4. Bers DM. Calcium cycling and signaling in cardiac myocytes. *Annu Rev Physiol*. 2008;70:23-49.

5. Beavo JA, Francis SH and Houslay MD. Cyclic nucleotide phosphodiesterases in health and diseases. *CRC Press, Taylor & Francis Group, Boca Raton, Florida, USA*. 2007.

6. Leroy J, Abi-Gerges A, Nikolaev VO, Richter W, Lechene P, Mazet JL, Conti M, Fischmeister R and Vandecasteele G. Spatiotemporal dynamics of beta-adrenergic cAMP signals and L-type Ca2+ channel regulation in adult rat ventricular myocytes: role of phosphodiesterases. *Circ Res*. 2008;102:1091-100.

7. Molina CE, Johnson DM, Mehel H, Spatjens RL, Mika D, Algalarrondo V, Slimane ZH, Lechene P, Abi-Gerges N, van der Linde HJ, Leroy J, Volders PG, Fischmeister R and Vandecasteele G. Interventricular Differences in beta-Adrenergic Responses in the Canine Heart: Role of Phosphodiesterases. *J Am Heart Assoc*. 2014;3.

8. Mika D, Bobin P, Lindner M, Boet A, Hodzic A, Lefebvre F, Lechene P, Sadoune M, Samuel JL, Algalarrondo V, Rucker-Martin C, Lambert V, Fischmeister R, Vandecasteele G and Leroy J. Synergic PDE3 and PDE4 control intracellular cAMP and cardiac excitation-contraction coupling in a porcine model. *J Mol Cell Cardiol*. 2019;133:57-66.

9. Molina CE, Leroy J, Richter W, Xie M, Scheitrum C, Lee IO, Maack C, Rucker-Martin C, Donzeau-Gouge P, Verde I, Llach A, Hove-Madsen L, Conti M, Vandecasteele G and Fischmeister R. Cyclic adenosine monophosphate phosphodiesterase type 4 protects against atrial arrhythmias. *J Am Coll Cardiol*. 2012;59:2182-90.

10. Bobin P, Varin A, Lefebvre F, Fischmeister R, Vandecasteele G and Leroy J. Calmodulin kinase II inhibition limits the pro-arrhythmic Ca2+ waves induced by cAMP-phosphodiesterase inhibitors. *Cardiovasc Res*. 2016;110:151-61.

11. Zoccarato A, Surdo NC, Aronsen JM, Fields LA, Mancuso L, Dodoni G, Stangherlin A, Livie C, Jiang H, Sin YY, Gesellchen F, Terrin A, Baillie GS, Nicklin SA, Graham D, Szabo-Fresnais N, Krall J, Vandeput F, Movsesian M, Furlan L, Corsetti V, Hamilton G, Lefkimmiatis K, Sjaastad I and Zaccolo M. Cardiac Hypertrophy Is Inhibited by a Local Pool of cAMP Regulated by Phosphodiesterase 2. *Circ Res*. 2015;117:707-19.

12. Richter W, Xie M, Scheitrum C, Krall J, Movsesian MA and Conti M. Conserved expression and functions of PDE4 in rodent and human heart. *Basic Res Cardiol*. 2011;106:249-62.

13. Lehnart SE, Wehrens XH, Reiken S, Warrier S, Belevych AE, Harvey RD, Richter W, Jin SL, Conti M and Marks AR. Phosphodiesterase 4D deficiency in the ryanodine-receptor complex promotes heart failure and arrhythmias. *Cell*. 2005;123:25-35.

14. Beca S, Helli PB, Simpson JA, Zhao D, Farman GP, Jones PP, Tian X, Wilson LS, Ahmad F, Chen SR, Movsesian MA, Manganiello V, Maurice DH, Conti M and Backx PH. Phosphodiesterase 4D regulates baseline sarcoplasmic reticulum Ca2+ release and cardiac contractility, independently of L-type Ca2+ current. *Circ Res*. 2011;109:1024-30.

15. Leroy J, Richter W, Mika D, Castro LR, Abi-Gerges A, Xie M, Scheitrum C, Lefebvre F, Schittl J, Mateo P, Westenbroek R, Catterall WA, Charpentier F, Conti M, Fischmeister R and Vandecasteele G. Phosphodiesterase 4B in the cardiac L-type Ca2+ channel complex regulates Ca2+ current and protects against ventricular arrhythmias in mice. *J Clin Invest*. 2011;121:2651-61.

16. Abi-Gerges A, Richter W, Lefebvre F, Mateo P, Varin A, Heymes C, Samuel JL, Lugnier C, Conti M, Fischmeister R and Vandecasteele G. Decreased expression and activity of cAMP phosphodiesterases in cardiac hypertrophy and its impact on beta-adrenergic cAMP signals. *Circ Res*. 2009;105:784-92.

17. Mika D, Richter W, Westenbroek RE, Catterall WA and Conti M. PDE4B mediates local feedback regulation of beta(1)-adrenergic cAMP signaling in a sarcolemmal compartment of cardiac myocytes. *J Cell Sci*. 2014;127:1033-42.

18. Frey N, Frank D, Lippl S, Kuhn C, Kogler H, Barrientos T, Rohr C, Will R, Muller OJ, Weiler H, Bassel-Duby R, Katus HA and Olson EN. Calsarcin-2 deficiency increases exercise capacity in mice through calcineurin/NFAT activation. *J Clin Invest*. 2008;118:3598-608.

19. Nakamura M and Sadoshima J. Mechanisms of physiological and pathological cardiac hypertrophy. *Nat Rev Cardiol*. 2018;15:387-407.

20. Klarenbeek J, Goedhart J, van Batenburg A, Groenewald D and Jalink K. Fourth-Generation Epac-Based FRET Sensors for cAMP Feature Exceptional Brightness, Photostability and Dynamic Range: Characterization of Dedicated Sensors for FLIM, for Ratiometry and with High Affinity. *PLoS One*. 2015;10:e0122513.

21. Allen MD and Zhang J. Subcellular dynamics of protein kinase A activity visualized by FRET-based reporters. *Biochem Biophys Res Commun*. 2006;348:716-21.

22. Molenaar P, Christ T, Hussain RI, Engel A, Berk E, Gillette KT, Chen L, Galindo-Tovar A, Krobert KA, Ravens U, Levy FO and Kaumann AJ. PDE3, but not PDE4, reduces beta(1) - and beta(2)-adrenoceptor-mediated inotropic and lusitropic effects in failing ventricle from metoprolol-treated patients. *Br J Pharmacol*. 2013;169:528-38.

23. Molenaar P, Christ T, Berk E, Engel A, Gillette KT, Galindo-Tovar A, Ravens U and Kaumann AJ. Carvedilol induces greater control of beta2- than beta 1-adrenoceptor-mediated

inotropic and lusitropic effects by PDE3, while PDE4 has no effect in human failing myocardium. *Naunyn Schmiedebergs Arch Pharmacol*. 2014;387:629-40.

24. Ohtsuka M, Miura H, Mochida K, Hirose M, Hasegawa A, Ogura A, Mizutani R, Kimura M, Isotani A, Ikawa M, Sato M and Gurumurthy CB. One-step generation of multiple transgenic mouse lines using an improved Pronuclear Injection-based Targeted Transgenesis (i-PITT). *BMC Genomics*. 2015;16:274.

25. Galindo-Tovar A and Kaumann AJ. Phosphodiesterase-4 blunts inotropism and arrhythmias but not sinoatrial tachycardia of (-)-adrenaline mediated through mouse cardiac beta(1)-adrenoceptors. *Br J Pharmacol*. 2008;153:710-20.

26. Christ T, Galindo-Tovar A, Thoms M, Ravens U and Kaumann AJ. Inotropy and L-type Ca current, activated by beta- and beta-adrenoceptors, are differently controlled by phosphodiesterases 3 and 4 in rat heart. *Br J Pharmacol*. 2009;156:62-83.

27. Nikolaev VO, Bunemann M, Schmitteckert E, Lohse MJ and Engelhardt S. Cyclic AMP imaging in adult cardiac myocytes reveals far-reaching beta1-adrenergic but locally confined beta2-adrenergic receptor-mediated signaling. *Circ Res*. 2006;99:1084-91.

28. Oikawa M, Wu M, Lim S, Knight WE, Miller CL, Cai Y, Lu Y, Blaxall BC, Takeishi Y, Abe J and Yan C. Cyclic nucleotide phosphodiesterase 3A1 protects the heart against ischemia-reperfusion injury. *J Mol Cell Cardiol*. 2013;64:11-9.

29. Ghigo A, Perino A, Mehel H, Zahradnikova AJ, Morello F, Leroy J, Nikolaev VO, Damilano F, Cimino J, De Luca E, Richter W, Westenbroek R, Catterall WA, Zhang J, Yan C, Conti M, Gomez AM, Vandecasteele G, Hirsch E and Fischmeister R. PI3Kgamma Protects against Catecholamine-Induced Ventricular Arrhythmia through PKA-mediated Regulation of Distinct Phosphodiesterases. *Circulation*. 2012;126:2073-83.

30. Vettel C, Lindner M, Dewenter M, Lorenz K, Schanbacher C, Riedel M, Lammle S, Meinecke S, Mason FE, Sossalla S, Geerts A, Hoffmann M, Wunder F, Brunner FJ, Wieland T, Mehel H, Karam S, Lechene P, Leroy J, Vandecasteele G, Wagner M, Fischmeister R and El-Armouche A. Phosphodiesterase 2 Protects Against Catecholamine-Induced Arrhythmia and Preserves Contractile Function After Myocardial Infarction. *Circ Res*. 2017;120:120-132.

31. Vinogradova TM, Lyashkov AE, Zhu W, Ruknudin AM, Sirenko S, Yang D, Deo S, Barlow M, Johnson S, Caffrey JL, Zhou YY, Xiao RP, Cheng H, Stern MD, Maltsev VA and Lakatta EG. High basal protein kinase A-dependent phosphorylation drives rhythmic internal Ca2+ store oscillations and spontaneous beating of cardiac pacemaker cells. *Circ Res*. 2006;98:505-14.

32. Rohrer DK, Schauble EH, Desai KH, Kobilka BK and Bernstein D. Alterations in dynamic heart rate control in the beta 1-adrenergic receptor knockout mouse. *Am J Physiol*. 1998;274:H1184-93.

33. Rohrer DK, Chruscinski A, Schauble EH, Bernstein D and Kobilka BK. Cardiovascular and metabolic alterations in mice lacking both beta1- and beta2-adrenergic receptors. *J Biol Chem*. 1999;274:16701-8.

34. Habouzit E, Richard H, Sanchez H, Koulmann N, Serrurier B, Monnet R, Ventura-Clapier R and Bigard X. Decreased muscle ACE activity enhances functional response to endurance training in rats, without change in muscle oxidative capacity or contractile phenotype. *J Appl Physiol (1985)*. 2009;107:346-53.

35. Ladage D, Schwinger RH and Brixius K. Cardio-selective beta-blocker: pharmacological evidence and their influence on exercise capacity. *Cardiovasc Ther*. 2013;31:76-83.

36. Eto Y, Yonekura K, Sonoda M, Arai N, Sata M, Sugiura S, Takenaka K, Gualberto A, Hixon ML, Wagner MW and Aoyagi T. Calcineurin is activated in rat hearts with physiological left ventricular hypertrophy induced by voluntary exercise training. *Circulation*. 2000;101:2134-7.

37. Chung E, Yeung F and Leinwand LA. Calcineurin activity is required for cardiac remodelling in pregnancy. *Cardiovasc Res*. 2013;100:402-10.

38. Molkentin JD, Lu JR, Antos CL, Markham B, Richardson J, Robbins J, Grant SR and Olson EN. A calcineurin-dependent transcriptional pathway for cardiac hypertrophy. *Cell*. 1998;93:215-28.

39. Li XM, Ma YT, Yang YN, Liu F, Chen BD, Han W, Zhang JF and Gao XM. Downregulation of survival signalling pathways and increased apoptosis in the transition of pressure overload-induced cardiac hypertrophy to heart failure. *Clin Exp Pharmacol Physiol*. 2009;36:1054-61.

40. Sussman MA, Volkers M, Fischer K, Bailey B, Cottage CT, Din S, Gude N, Avitabile D, Alvarez R, Sundararaman B, Quijada P, Mason M, Konstandin MH, Malhowski A, Cheng Z, Khan M and McGregor M. Myocardial AKT: the omnipresent nexus. *Physiol Rev*. 2011;91:1023-70.

41. DeBosch B, Treskov I, Lupu TS, Weinheimer C, Kovacs A, Courtois M and Muslin AJ. Akt1 is required for physiological cardiac growth. *Circulation*. 2006;113:2097-104.

42. Brancaccio M, Fratta L, Notte A, Hirsch E, Poulet R, Guazzone S, De Acetis M, Vecchione C, Marino G, Altruda F, Silengo L, Tarone G and Lembo G. Melusin, a muscle-specific integrin beta1-interacting protein, is required to prevent cardiac failure in response to chronic pressure overload. *Nat Med*. 2003;9:68-75.

43. Benard L, Oh JG, Cacheux M, Lee A, Nonnenmacher M, Matasic DS, Kohlbrenner E, Kho C, Pavoine C, Hajjar RJ and Hulot JS. Cardiac Stim1 Silencing Impairs Adaptive Hypertrophy and Promotes Heart Failure Through Inactivation of mTORC2/Akt Signaling. *Circulation*. 2016;133:1458-71.

44. Benjamin IJ, Jalil JE, Tan LB, Cho K, Weber KT and Clark WA. Isoproterenol-induced myocardial fibrosis in relation to myocyte necrosis. *Circ Res*. 1989;65:657-70.

45. Zhao L, Cheng G, Jin R, Afzal MR, Samanta A, Xuan YT, Girgis M, Elias HK, Zhu Y, Davani A, Yang Y, Chen X, Ye S, Wang OL, Chen L, Hauptman J, Vincent RJ and Dawn B. Deletion of Interleukin-6 Attenuates Pressure Overload-Induced Left Ventricular Hypertrophy and Dysfunction. *Circ Res*. 2016;118:1918-1929.

46. Communal C, Singh K, Pimentel DR and Colucci WS. Norepinephrine stimulates apoptosis in adult rat ventricular myocytes by activation of the beta-adrenergic pathway. *Circulation*. 1998;98:1329-34.

47. Nakayama H, Chen X, Baines CP, Klevitsky R, Zhang X, Zhang H, Jaleel N, Chua BH, Hewett TE, Robbins J, Houser SR and Molkentin JD. Ca2+- and mitochondrial-dependent cardiomyocyte necrosis as a primary mediator of heart failure. *J Clin Invest*. 2007;117:2431-44.

48. Yang Y, Zhu WZ, Joiner ML, Zhang R, Oddis CV, Hou Y, Yang J, Price EE, Gleaves L, Eren M, Ni G, Vaughan DE, Xiao RP and Anderson ME. Calmodulin kinase II inhibition protects against myocardial cell apoptosis in vivo. *Am J Physiol Heart Circ Physiol*. 2006;291:H3065-75.

49. Liggett SB, Tepe NM, Lorenz JN, Canning AM, Jantz TD, Mitarai S, Yatani A and Dorn GWn. Early and delayed consequences of beta(2)-adrenergic receptor overexpression in mouse hearts: critical role for expression level. *Circulation*. 2000;101:1707-14.

50. Omar F, Findlay JE, Carfray G, Allcock RW, Jiang Z, Moore C, Muir AL, Lannoy M, Fertig BA, Mai D, Day JP, Bolger G, Baillie GS, Schwiebert E, Klussmann E, Pyne NJ, Ong ACM, Bowers K, Adam JM, Adams DR, Houslay MD and Henderson DJP. Small-molecule allosteric activators of PDE4 long form cyclic AMP phosphodiesterases. *Proc Natl Acad Sci U S A*. 2019;116:13320-13329.

FIGURE LEGENDS

Figure 1: PDE4B is decreased in human heart failure. A, Western blot analysis of PDE4B expression in total protein extracts from non-failing (N=7) and failing (N=7) hearts of ischemic origin. B, Western blot analysis of PDE4B expression in total protein extracts from non-failing (N=5) and failing (N=5) hearts with dilated cardiomyopathy. Human tissues were collected from two different Parisian hospitals in A and B. β-actin was used as loading control. Bars represent the mean ± SEM. **P*<0.05, ***P*<0.01, Mann-Whitney test.

Figure 2: Cardiac phenotype of transgenic mice with cardiac-specific PDE4B overexpression, TG15 line. A, PDE4B mRNA expression in WT (N=7) and TG15 (N=9) hearts measured by qRT-PCR. B, PDE4B protein expression in WT (N=8) and TG15 (N=7) hearts measured by Western blot. For WT, 20 µg protein were loaded whereas 2 µg were loaded for TG. Calsequestrin (CSQ) was used as a loading control. C, Total cAMP-PDE activity and D, PDE4 specific activity in heart extracts from WT (N=8) and TG15 (N=7) mice measured by radioenzymatic assay with 1 µmol/L cAMP as substrate. E, cAMP content in cardiac extracts from WT (N=8) and TG15 (N=9) hearts. F, Representative echocardiographic M-mode images, fractional shortening (FS), heart rate, end-diastolic left ventricular internal diameter (LVIDd) and left ventricular weight (LVW) to body weight (BW) ratio evaluated by echocardiography in anesthetized WT (N=20) and TG15 (N=26) mice. G, Heart weight (HW) and lung weight (LW) normalized to tibia length (TL) in WT (N=14) and TG15 mice (N=19). H-J, Western blot analysis of total protein extracts from WT (N=8) and TG15 mice (N=8) cardiac ventricles using antibodies for phospho-PLB (P-PLB) (H), phospho-TnI (P-TnI) (I) and phospho-myosin-binding protein C (P-MyBP-C) (J). Representative blots are shown, and phosphorylated/total protein ratios were quantified and expressed as mean ± SEM. **P*<0.05, ***P*<0.01, ****P*<0.001, Mann-Whitney test (A-E), Student t-test (F-J).

Figure 3: Long term consequences of PDE4B cardiac overexpression depend on expression level. A, Evolution of cardiac structure and function assessed by serial echocardiography in WT mice (white diamonds), TG15 mice (black triangles) and TG50 mice (red squares) during aging. Mean values ± SEM of heart rate, fractional shortening (FS), end-diastolic left ventricular internal diameter (LVIDd), calculated left ventricle weight (LVW) and LVW normalized to body weight (LVW/BW) are shown. **P*<0.05, ***P*<0.01, ****P*<0.001 *versus* WT. $^{\$\$}$*P*<0.05, between TG15 and TG50. Two-way, mixed-effects ANOVA with Tukey's multiple comparison test. B, Mean values (± SEM) of measured heart weight (HW) and lung weight (LW) normalized to body weight (BW) and tibia length (TL) obtained from WT, TG15 and TG50 mice (average age 59 weeks). ****P*<0.001 *versus* WT and TG15. Kruskal-Wallis with Dunn's multiple comparisons test (HW/TL) or ordinary one-way ANOVA with Tukey's multiple comparisons test (HW/BW, LW/BW and LW/TL). C, Kaplan-Meier plot of survival in WT, TG15 and TG50. A Log rank test was used to compare the survival curves. Number of mice is indicated in brackets in the legend.

Figure 4: PDE4B-TG15 mice have attenuated responses to isoproterenol *in vivo* and in isolated perfused hearts. A, B, Anesthetized WT (N=6) and TG15 (N=6) mice were subjected to an intra-peritoneal Iso injection (0.02 mg/kg); fractional shortening (FS) and heart rate were measured by echocardiography and 6-lead ECG respectively, at baseline and 2 minutes after injection. C, D, Developed pressure and heart rate measured in Langendorff-perfused hearts at baseline (N=4 per group). E, Concentration-response curves to isoproterenol (Iso) on developed pressure in WT and TG15 hearts paced at 650 bpm (N=4 per group). F, EC_{50} values deduced from curves obtained in E. ***P*<0.01, ****P*<0.001 between basal and Iso, $^{\$\$}$*P*<0.01 between WT and TG15 (A, B). **P*<0.05 between WT and TG15 (E, F). Two-way, mixed effects ANOVA with Sidak's multiple comparison test (A, B, E), Mann-Whitney test (C, D, F).

Figure 5: Decreased inotropic, lusitropic and pro-arrhythmic effects of isoproterenol in isolated ventricular myocytes from PDE4B-TG15 mice. A, Representative traces of sarcomere shortening

(top) and Ca^{2+} transients (bottom) in paced (0.5 Hz) ventricular myocytes isolated from WT (grey traces) and TG15 mice (black traces) in control conditions (left panels) and in the presence of 100 nmol/L isoproterenol (right panels). B, Concentration-response curves of Iso on sarcomere shortening (expressed as the percentage of resting sarcomere length) in WT and TG15 myocytes. Both curves were different (extra sum-of-squares F test) with statistically different E_{max} (***P<0.001, Student t-test) and EC_{50} values (*P<0.05, Student t-test). C, Average $t_{1/2}$ values for sarcomere relaxation at 100 nmol/L Iso; D, Concentration-response curves of Iso on Ca^{2+} transient amplitude (expressed as the percentage of diastolic Fura-2 ratio) in WT and TG15 myocytes. Both curves were different (extra sum-of-squares F test) with statistically different E_{max} (*P<0.05). E, Average $t_{1/2}$ values for Ca^{2+} transient decay at 100 nmol/L Iso. Responses to Iso were measured in 12-24 cells from 6 WT and 12-26 cells from 7 TG15 mice. F, Representative traces of spontaneous Ca^{2+} release events (SCRs, arrow heads) induced by Iso (100 nmol/L) in a WT and a TG15 cardiomyocyte. Vertical bars indicate electrical pacing at 0.5 Hz. G, Average number (± SEM) of SCRs during a 10-second period after the peak of the Iso effect in WT (N=5, n=22, white bars) and TG15 (N=5, n=28, black bars). H, Number of cells (WT and TG15) with and without SCRs in the absence and presence of Iso. *P<0.05, **P<0.01, ***P<0.001, Mann-Whitney test (C, E), Two-way ANOVA with Sidak's multiple comparison test (G), Fisher's exact test (H).

Figure 6: PDE4B-TG15 mice are protected against maladaptive remodeling induced by chronic isoproterenol infusion A, Schematic representation of the experimental protocol. WT and TG15 mice were implanted subcutaneously with osmotic minipumps diffusing 60 mg/kg/day of Iso or vehicle solution (0.9% NaCl) during 2 weeks (hatched bar) and kept for 2 additional weeks before sacrifice. Cardiac function was evaluated by echocardiography before, and 2 and 4 weeks after the minipump implantation. B, Time course of fractional shortening (FS) and calculated left ventricular weight (LVW) to body weight (BW) ratio normalized to the first echocardiography at 0 week in WT and PDE4B-TG mice treated with 0.9% NaCl (black) or Iso (red). Number of mice per group are

indicated in brackets above the graphs. C, Average heart weight (HW) and lung weight (LW) to tibia length (TL) ratios in WT and TG15 mice treated with NaCl (black) or Iso (red). Error bars represent SEM and number of mice is indicated inside the bars. D, Representative images of Masson's trichrome staining (scale bar 100 µm) and quantification of interstitial fibrosis in WT and TG15 mice treated with NaCl (black) or Iso (red). In C, number of mice is indicated inside the bars. Graphs represent the mean ± SEM. Statistical significance between WT Iso and WT NaCl is indicated by **P*<0.05, ***P*<0.01, ****P*<0.001; TG Iso *vs* TG NaCl by $^{\$}$*P*<0.05, $^{\$\$\$}$*P*<0.001; TG Iso *vs* WT Iso by $^{\#\#}$*P*<0.01. Two-way, mixed effects ANOVA with Tukey's multiple comparison test (B). Two-way ANOVA with Sidak's multiple comparison test (C, D).

Figure 7: Gene therapy with PDE4B protects against maladaptive remodeling induced by chronic isoproterenol treatment. A, Schematic representation of the experimental protocol. Mice were injected with AAV9 encoding luciferase (AAV9-Luc) or PDE4B (AAV9-PDE4B). Two weeks later, AAV9-Luc mice were implanted subcutaneously with osmotic minipumps diffusing 60 mg/kg/day of Iso (Luc-Iso) or vehicle solution (Luc-NaCl) while AAV9-PDE4B mice were implanted only with minipumps delivering Iso (PDE4B-Iso). Treatment duration was 2 weeks (hatched bars). Mice were kept for 2 additional weeks prior to sacrifice. Cardiac function was evaluated by echocardiography before AAV injection (0 week) and at 2, 4, 5 and 6 weeks. B, Time course of average fractional shortening (FS) and calculated left ventricular weight (LVW) to body weight (BW) ratio in Luc-NaCl, Luc-Iso and PDE4B-Iso mice. Number of mice is indicated in brackets in the legend. C, Mean ± SEM of heart (HW) and lung weight (LW) to tibia length (TL) ratios in the three groups. D, *Top*, representative images of Masson's trichrome staining (scale bar 100 µm); *Bottom,* representative images of TUNEL assay (scale bar 20 µm) to detect apoptotic nuclei (green) co-stained with the glycocalix marker wheat germ agglutinin (red) and Hoechst (blue). E, Quantification of interstitial fibrosis and apoptotic nuclei in Luc-NaCl, Luc-Iso and PDE4B-Iso mice. In C and E, the

bar graphs represent the mean ± SEM. In C, the number of mice is indicated inside the bars. Statistical significance between Luc-Iso or PDE4B-Iso *vs* Luc-NaCl is indicated by **P*<0.05, ***P*<0.01, ****P*<0.001; PDE4B-Iso *vs* Luc-Iso by $^{\$}$*P*<0.05, $^{\$\$}$*P*<0.01, $^{\$\$\$}$*P*<0.001. Two-way, mixed effects ANOVA with Tukey's multiple comparison test (B). One-way ANOVA with Holm-Sidak's or Dunn's multiple comparison tests when appropriate (C, E).

Figure 8: Gene therapy with PDE4B protects against maladaptive remodeling induced by pressure overload. A, Schematic representation of the experimental protocol. Mice were injected with AAV9 encoding for luciferase (AAV9-Luc) or PDE4B (AAV9-PDE4B) two days after TAC surgery (TAC-Luc or TAC-PDE4B). Sham-operated mice were only injected with AAV9-Luc (Sham-Luc). Cardiac function was evaluated by serial echocardiography before surgery as well as 2, 14, 35, and 42 days after surgery. B, Time course of average fractional shortening (FS) and calculated left ventricular weight (LVW) to body weight (BW) ratio in Sham-Luc, TAC-Luc and TAC-PDE4B mice. Number of mice is indicated in brackets in the legend. C, Mean heart (HW) and lung weight (LW) to tibia length (TL) ratios in Sham-Luc, TAC-Luc and TAC-PDE4B mice. D, *Top*, representative images of Masson's trichrome staining (scale bar 100 µm); *Bottom*, representative images of TUNEL assay (scale bar 25 µm) to detect apoptotic nuclei (green) co-stained with the glycocalix marker wheat germ agglutinin (red) and Hoechst (blue). E, Quantification of interstitial fibrosis and apoptotic nuclei in Sham-Luc, TAC-Luc and TAC-PDE4B hearts. In C and E, the bar graphs represent the mean ± SEM. In C the number of mice is indicated inside the bars. Statistical significance between TAC-Luc or TAC-PDE4B *vs* Sham-Luc is indicated by **P*<0.05, ***P*<0.01, ****P*<0.001; TAC-PDE4B *vs* TAC-Luc by $^{\$}$*P*<0.05, $^{\$\$\$}$*P*<0.001. Two-way, mixed effects ANOVA with Tukey's multiple comparison test (B), One-way ANOVA with Sidak's multiple comparison test or Dunn's multiple comparison test when appropriate (C, E).

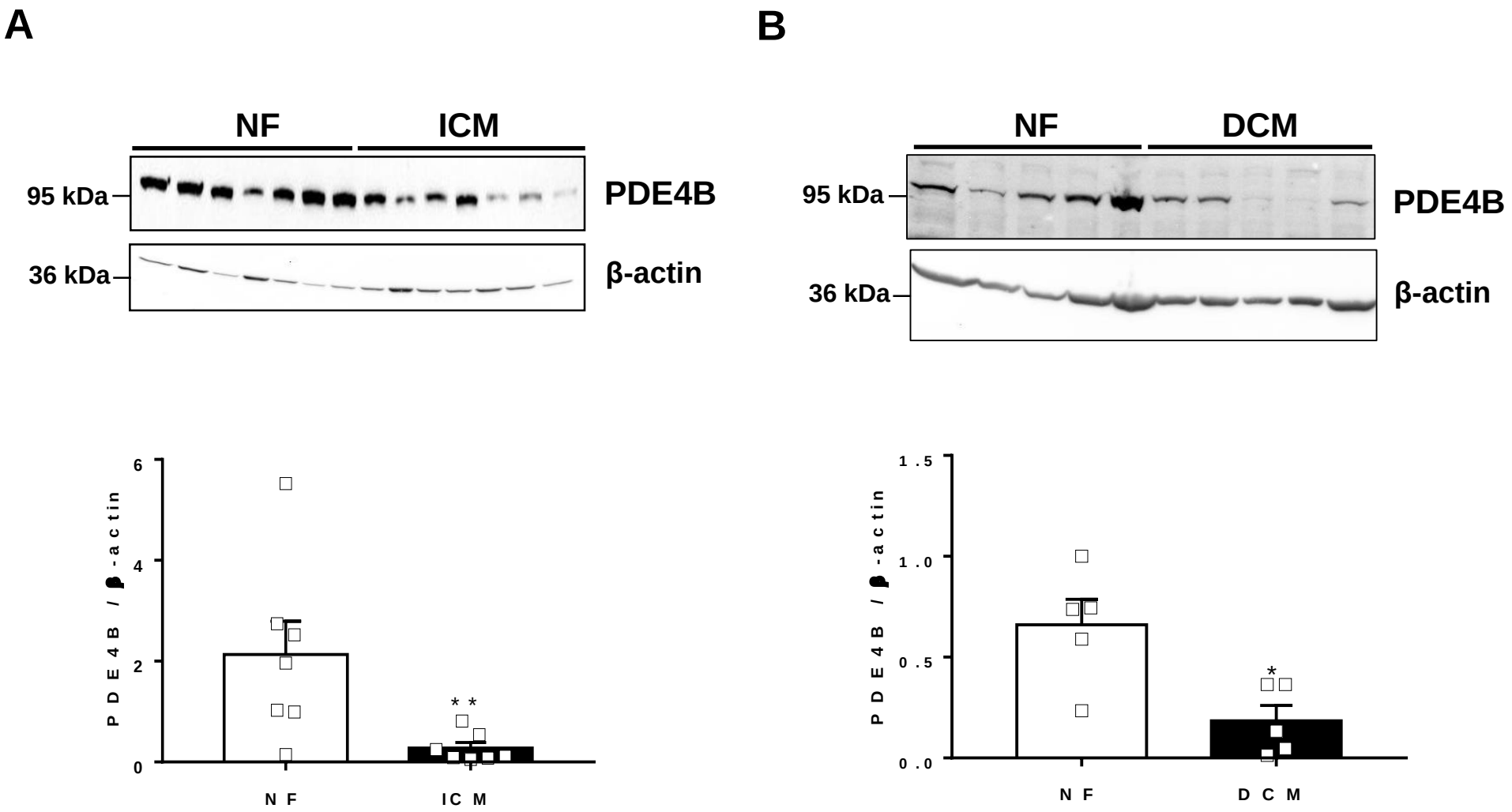
A
NF
ICM
95 kDa
PDE4B
36 kDa
β-actin
PDE4B / β-actin
6
4
2
0
**
NF
ICM
B
NF
DCM
95 kDa
PDE4B
36 kDa
β-actin
PDE4B / β-actin
1.5
1.0
0.5
0.0
*
NF
DCM

Figure 1

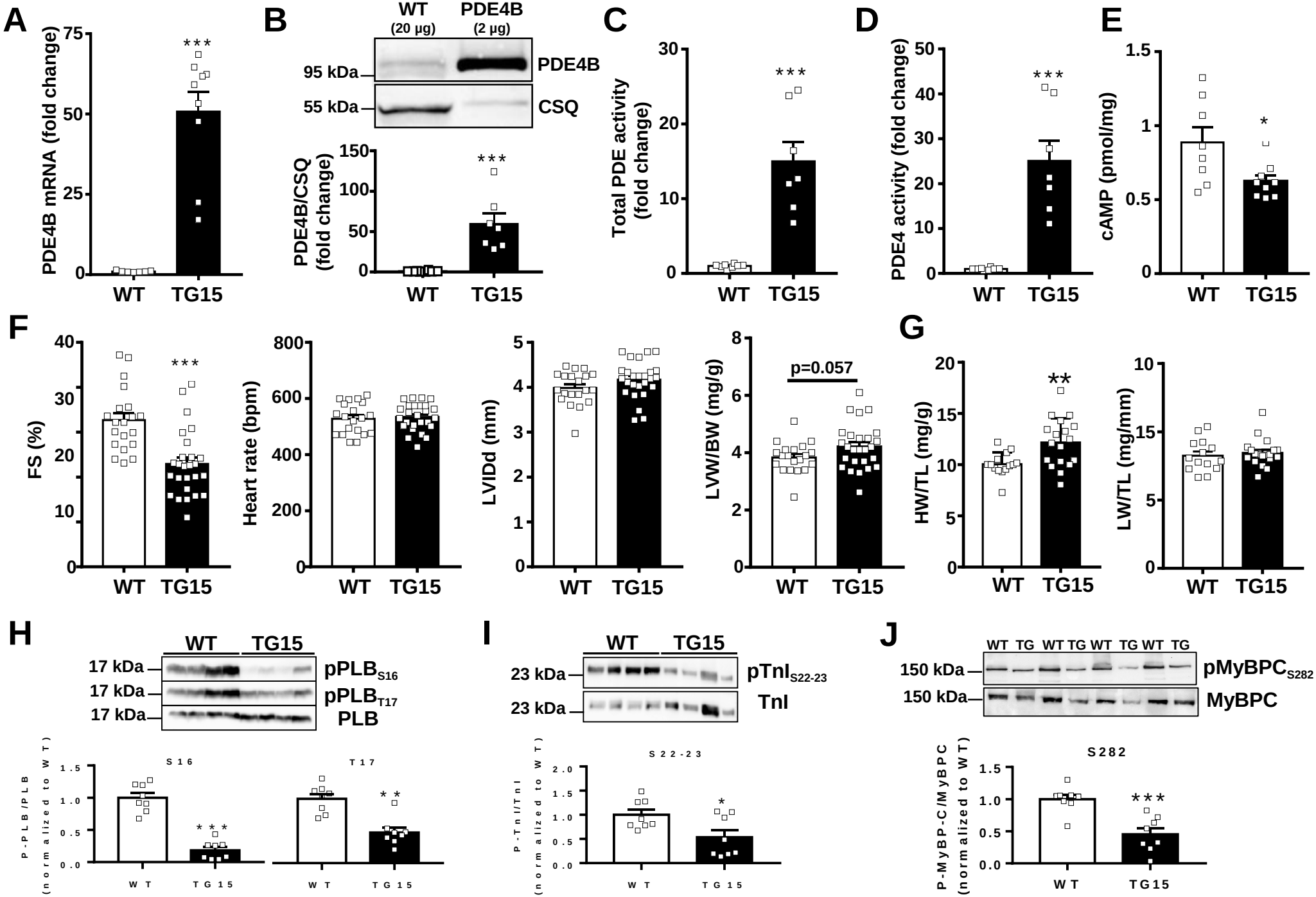
A
PDE4B mRNA (fold change)
75
50
25
0
***
WT
TG15
B
WT
(20 µg)
PDE4B
(2 µg)
95 kDa
PDE4B
55 kDa
CSQ
PDE4B/CSQ
(fold change)
150
100
50
0
***
WT
TG15
C
Total PDE activity
(fold change)
30
20
10
0
***
WT
TG15
D
PDE4 activity (fold change)
50
40
30
20
10
0
***
WT
TG15
E
cAMP (pmol/mg)
1.5
1
0.5
0
*
WT
TG15
F
FS (%)
40
30
20
10
0
***
WT
TG15
Heart rate (bpm)
800
600
400
200
0
WT
TG15
LVIDd (mm)
5
4
3
2
1
0
WT
TG15
LVW/BW (mg/g)
8
6
4
2
p=0.057
WT
TG15
G
HW/TL (mg/g)
20
15
10
5
0
**
WT
TG15
LW/TL (mg/mm)
10
15
5
0
WT
TG15
H
WT
TG15
17 kDa
pPLB$_{S16}$
17 kDa
pPLB$_{T17}$
17 kDa
PLB
P-PLB/PLB
(normalized to WT)
S16
1.5
1.0
0.5
0.0
***
WT
TG15
T17
**
WT
TG15
I
WT
TG15
23 kDa
pTnI$_{S22-23}$
23 kDa
TnI
P-TnI/TnI
(normalized to WT)
S22-23
2.0
1.5
1.0
0.5
0.0
*
WT
TG15
J
WT TG WT TG WT TG WT TG
150 kDa
pMyBPC$_{S282}$
150 kDa
MyBPC
P-MyBP-C/MyBPC
(normalized to WT)
S282
1.5
1.0
0.5
0.0
***
WT
TG15

Figure 2

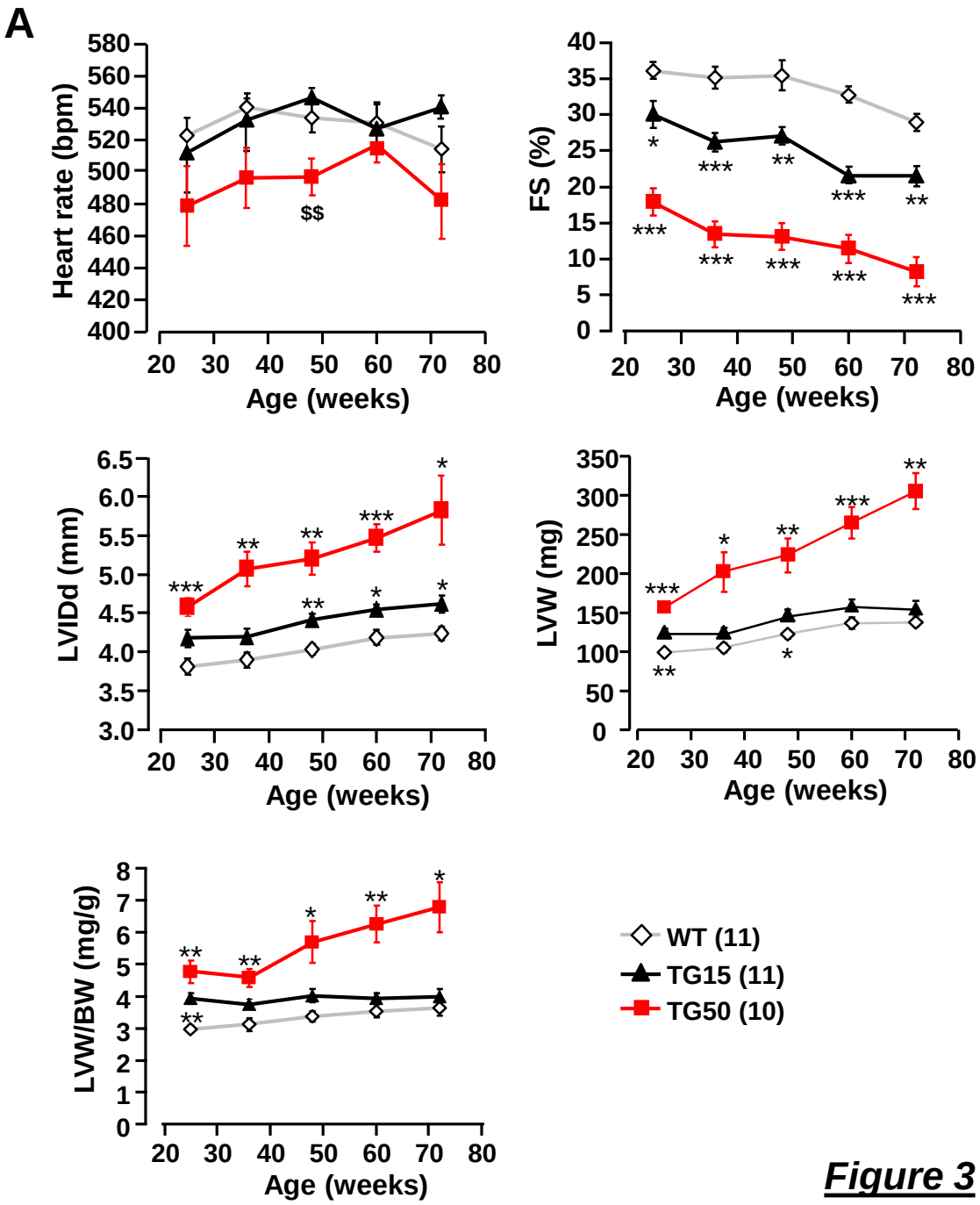
A
Heart rate (bpm)
Age (weeks)
$$
FS (%)
LVIDd (mm)
LVW (mg)
LVW/BW (mg/g)
WT (11)
TG15 (11)
TG50 (10)

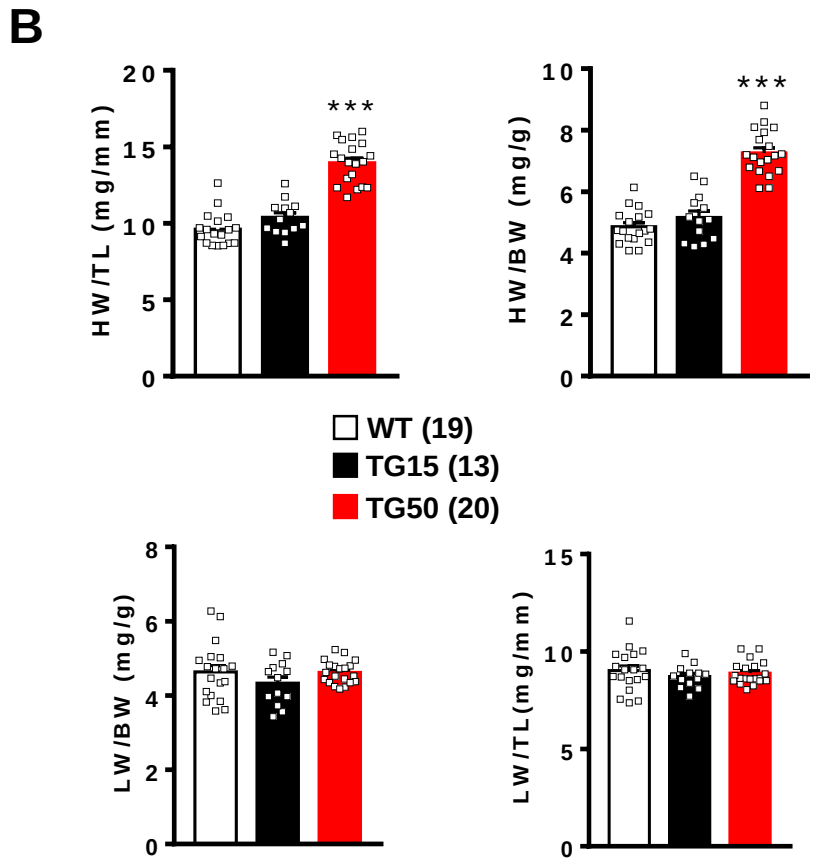
B
HW/TL (mg/mm)
HW/BW (mg/g)
WT (19)
TG15 (13)
TG50 (20)
LW/BW (mg/g)
LW/TL (mg/mm)

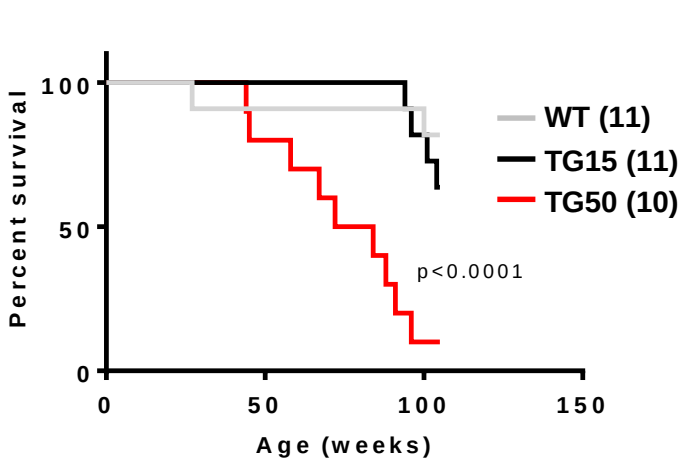
C
Percent survival
Age (weeks)
WT (11)
TG15 (11)
TG50 (10)
p<0.0001

Figure 3

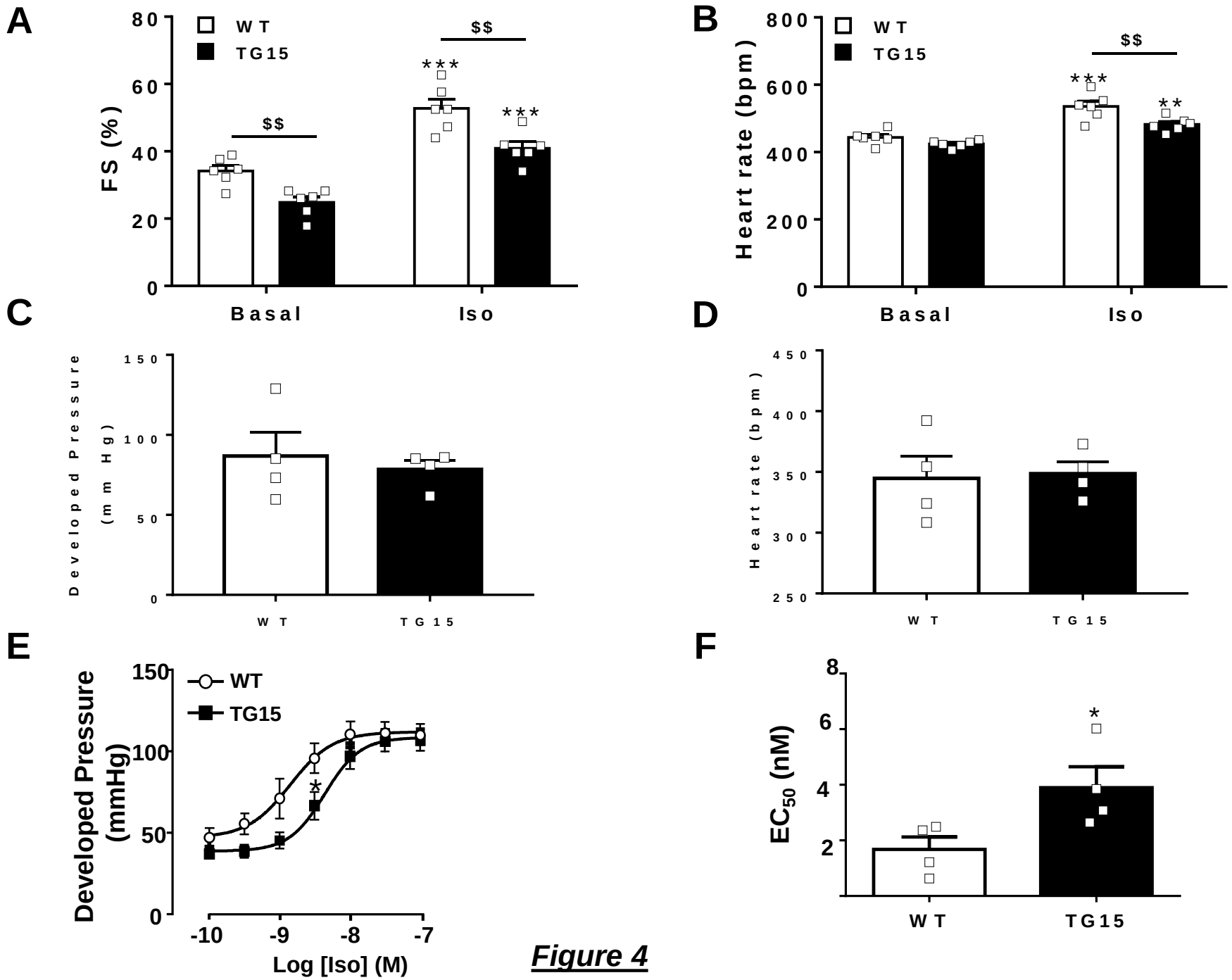
A
WT
TG15
FS (%)
80
60
40
20
0
$$
$$
***
***
Basal
Iso
B
WT
TG15
Heart rate (bpm)
800
600
400
200
0
$$
***
**
Basal
Iso
C
Developed Pressure (mm Hg)
150
100
50
0
WT
TG15
D
Heart rate (bpm)
450
400
350
300
250
WT
TG15
E
WT
TG15
Developed Pressure (mmHg)
150
100
50
0
*
-10
-9
-8
-7
Log [Iso] (M)
F
EC50 (nM)
8
6
4
2
*
WT
TG15

Figure 4

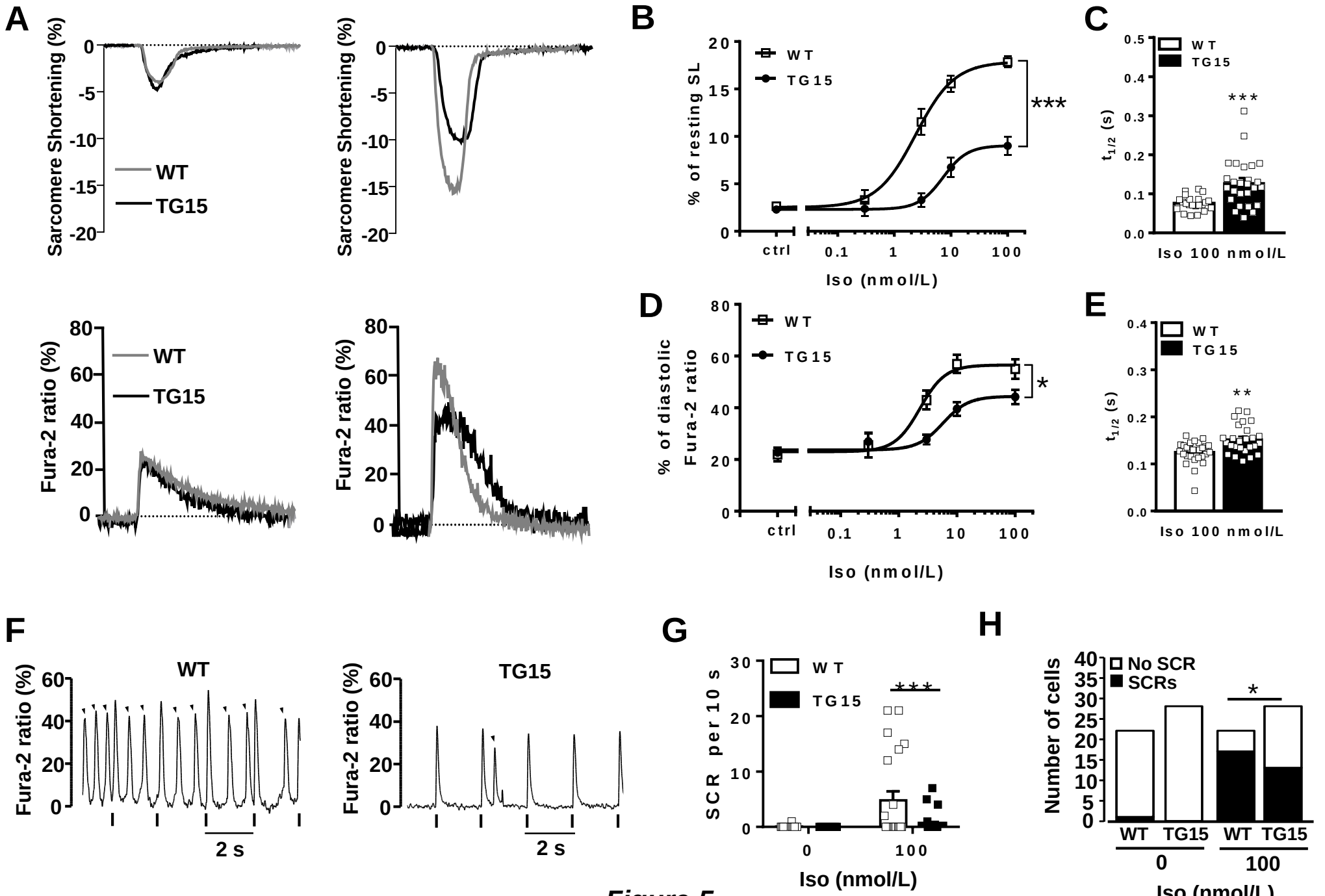
A
Sarcomere Shortening (%)
WT
TG15
Fura-2 ratio (%)
B
% of resting SL
Iso (nmol/L)
ctrl
***
C
$t_{1/2}$ (s)
Iso 100 nmol/L
D
% of diastolic Fura-2 ratio
*
E
F
2 s
G
SCR per 10 s
H
Number of cells
No SCR
SCRs

Figure 5

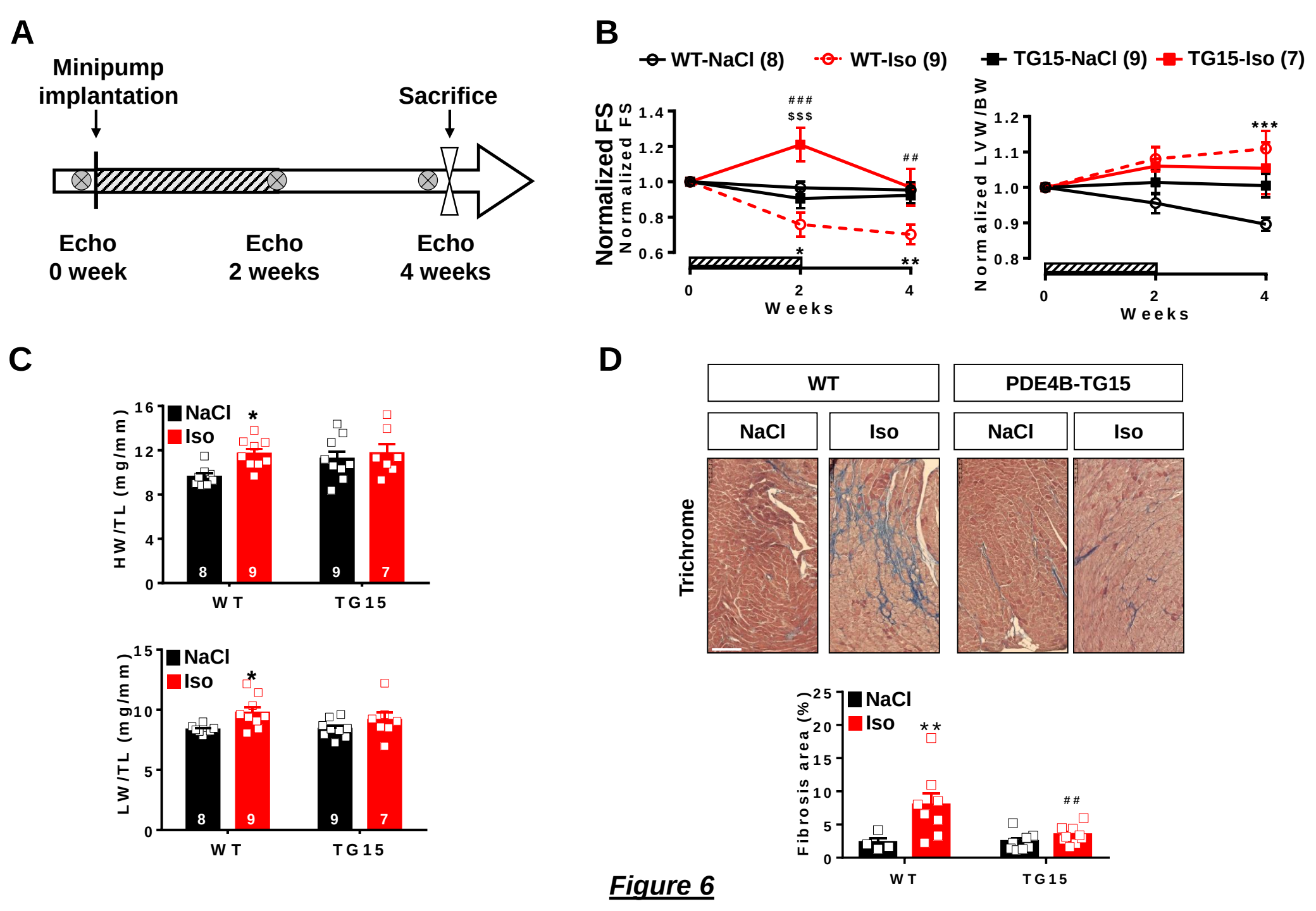
A
Minipump implantation
Sacrifice
Echo 0 week
Echo 2 weeks
Echo 4 weeks
B
WT-NaCl (8)
WT-Iso (9)
TG15-NaCl (9)
TG15-Iso (7)
Normalized FS
Normalized LVW/BW
Weeks
C
NaCl
Iso
HW/TL (mg/mm)
LW/TL (mg/mm)
WT
TG15
D
WT
PDE4B-TG15
NaCl
Iso
Trichrome
Fibrosis area (%)

Figure 6

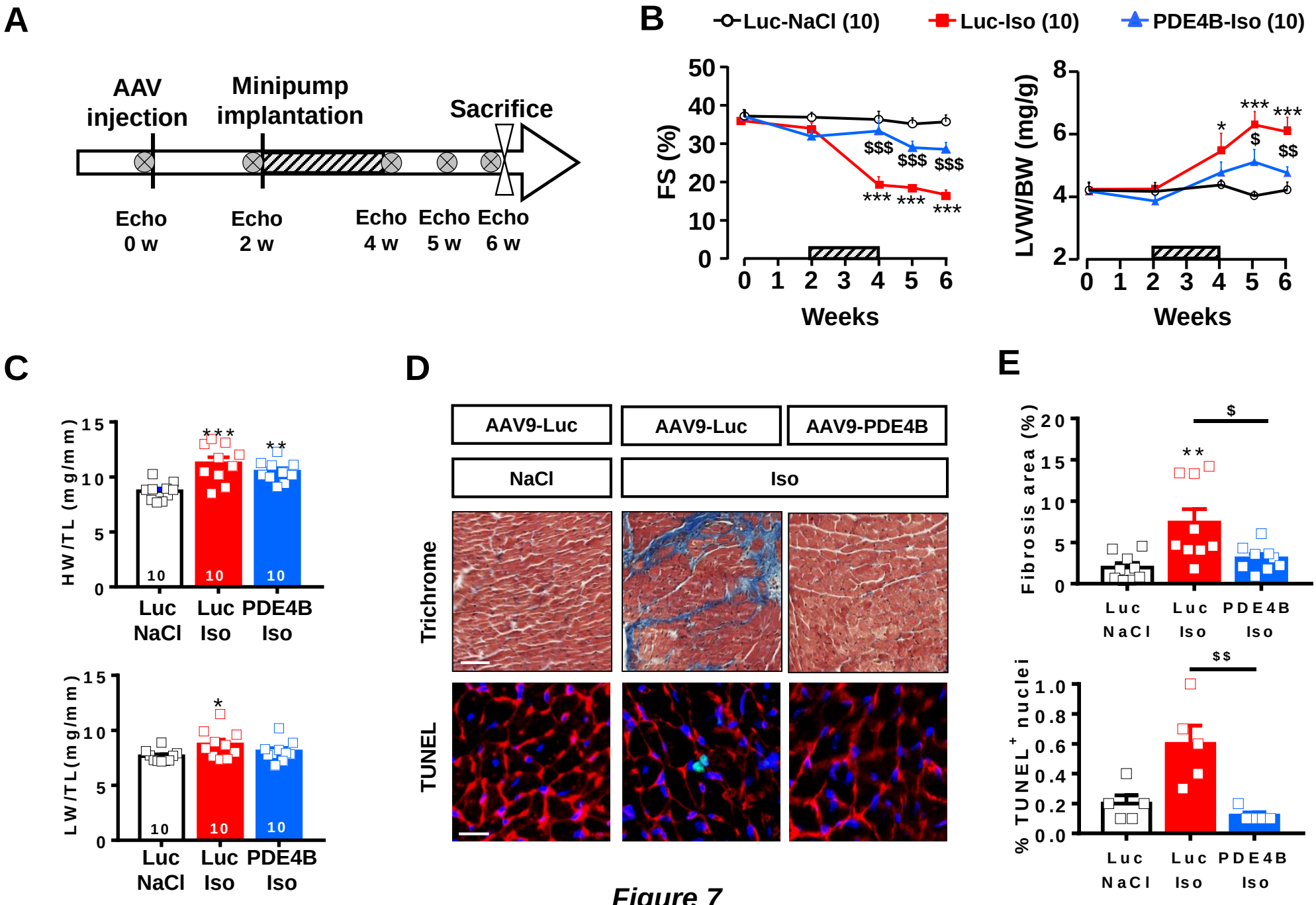
A
AAV injection
Minipump implantation
Sacrifice
Echo 0 w
Echo 2 w
Echo 4 w
Echo 5 w
Echo 6 w
B
Luc-NaCl (10)
Luc-Iso (10)
PDE4B-Iso (10)
FS (%)
Weeks
LVW/BW (mg/g)
Weeks
C
HW/TL (mg/mm)
LW/TL(mg/mm)
Luc NaCl
Luc Iso
PDE4B Iso
D
AAV9-Luc
AAV9-Luc
AAV9-PDE4B
NaCl
Iso
Trichrome
TUNEL
E
Fibrosis area (%)
% TUNEL+ nuclei

Figure 7

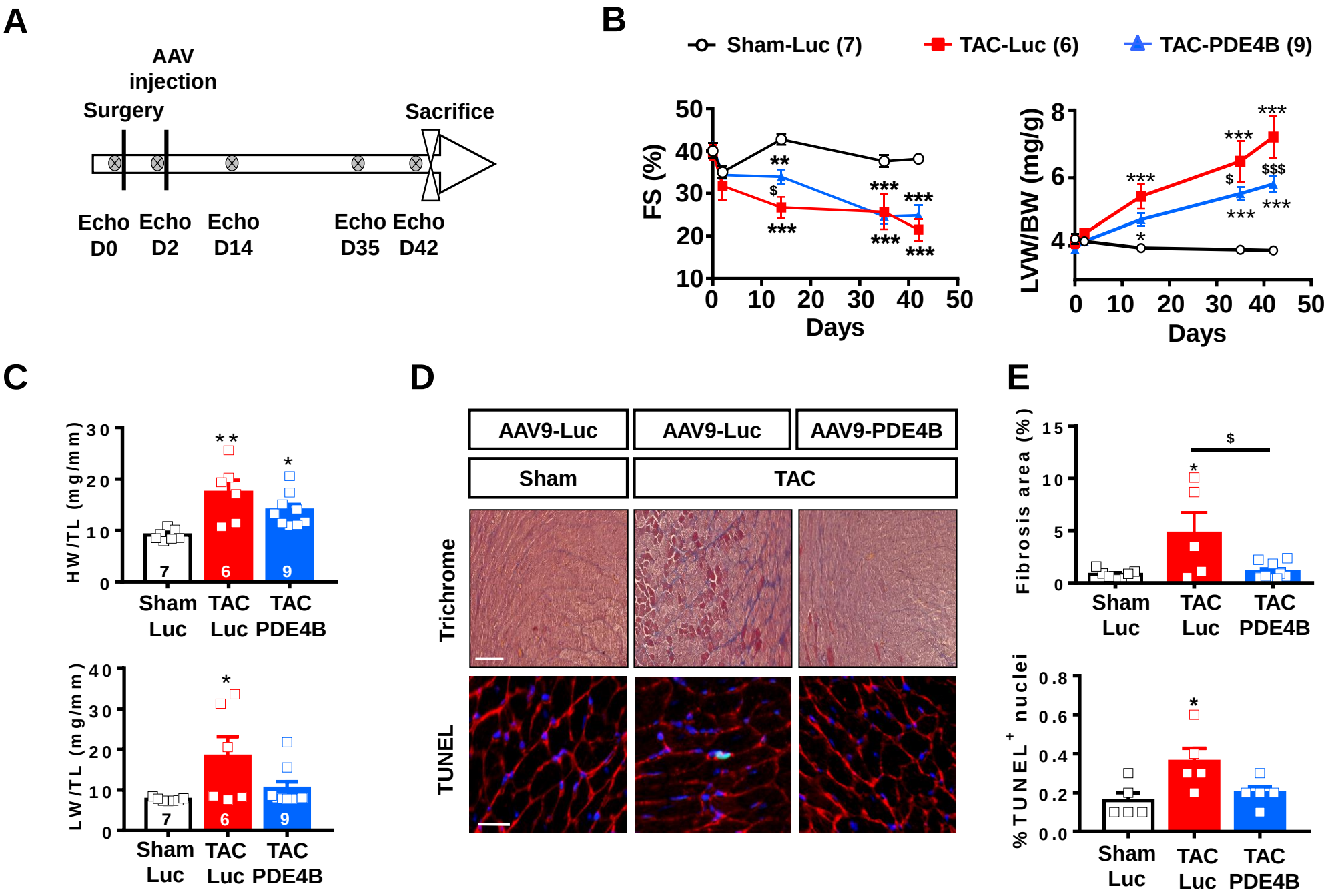
A
AAV injection
Surgery
Sacrifice
Echo D0
Echo D2
Echo D14
Echo D35
Echo D42
B
Sham-Luc (7)
TAC-Luc (6)
TAC-PDE4B (9)
FS (%)
Days
LVW/BW (mg/g)
Days
C
HW/TL (mg/mm)
LW/TL (mg/mm)
Sham Luc
TAC Luc
TAC PDE4B
D
AAV9-Luc
AAV9-Luc
AAV9-PDE4B
Sham
TAC
Trichrome
TUNEL
E
Fibrosis area (%)
% TUNEL+ nuclei
Sham Luc
TAC Luc
TAC PDE4B

Figure 8

SUPPLEMENTAL MATERIAL

Cardiac overexpression of PDE4B blunts β-adrenergic response and maladaptive remodeling in heart failure

Karam S[1]*, Margaria JP[2]*, Bourcier A[1]*, Mika D[1], Varin A[1], Bedioune I[1], Lindner M[1], Bouadjel K[1], Dessillons M[1], Gaudin F[3], Lefebvre F[1], Mateo P[1], Lechène P[1], Gomez S[1], Domergue V[3], Robert P[3], Coquard C[1], Algalarrondo V[1], Samuel JL[4], Michel JB[5], Charpentier F[6], Ghigo A[2], Hirsch E[2], Fischmeister R[1], Leroy J[1], Vandecasteele, G[1$]

[1]Université Paris-Saclay, Inserm, Signaling and Cardiovascular Pathophysiology, UMR-S 1180, 92296 Châtenay-Malabry, France.

[2]Department of Molecular Biotechnology and Health Sciences, Molecular Biotechnology Center, University di Torino, 10126 Torino, Italy.

[3]Université Paris-Saclay, Inserm, UMS-IPSIT, 92296 Châtenay-Malabry, France.

[4]UMR-S 942, INSERM, Paris University, 75010 Paris, France.

[5]UMR-S 1148, INSERM, Paris University, X. Bichat hospital, 75018 Paris, France.

[6]Institut du thorax, INSERM, CNRS, UNIV Nantes, 8 quai Moncousu, 44007 Nantes cedex 1, France.

Supplemental Methods

Reagents

Isoprenaline (Iso) was purchased from Sigma and Ro 20-1724 (Ro) was from Calbiochem.

Human heart tissue

Human heart tissue was obtained from the cardiovascular biobank of Bichat-Claude Bernard Hospital (BB-0033-00029, authorization AC-2018-3171 of the French Ministry of Research and Innovation, and PFS17-002 of the French Biomedicine Agency, coordinator Dr. JB Michel) and from a tissue collection from the Pitié-Salpétrière Hospital (coordinator Dr. Jane-Lise Samuel), with approval by the Inserm Institutional Review Board and the Consultative Committee for the Protection of Human Subjects in Biomedical Research at the Pitié-Salpétrière Hospital, respectively. The study was performed with left ventricular myocardium (LV) of end-stage failing hearts from patients with ischemic cardiomyopathy and idiopathic dilated cardiomyopathy. Non-failing LV was obtained from brain-dead organ donors that were unsuitable for transplantation for technical reasons. Patients or their relatives were informed that anonymized tissue will be used for research and given the right to refuse.

Transgenic mouse generation

Mice overexpressing PDE4B specifically in the heart (PDE4B-TG, C57/Bl6) were generated at the Institut Clinique de la Souris (Strasbourg, France). A mouse cDNA encoding for PDE4B3 (NCBI NM_019840.2, corresponding to mouse PDE4B transcript variant 1 in the NCBI nomenclature), kindly provided by Dr. J. Cherry (Boston University, Boston, MA, USA),[1] was subcloned between the 5.5-kb murine α-MHC promoter and the human growth hormone polyadenylation sequence of a pBluescript-based vector (a kind gift from Dr J. Robbins, Children's Hospital Research Foundation, Cincinnati, OH, USA).[2] The purified transgene

fragment was injected into pronuclei of fertilized mouse eggs and the injected eggs were surgically implanted into pseudopregnant females. Genotype of mouse pups was confirmed by PCR assay. To avoid potential confounding effects due to cyclic hormonal variations, only males were used in this study.

AAV9 vector production, purification, characterization and injection

AAV9-PDE4B carries a PDE4B expression cassette flanked by two AAV2 inverted terminal repeats. The expression sequence is pseudotyped with an AAV9 capsid. The PDE4B expression cassette contains a CMV promoter, a β-globin intron, a FLAG tag fused in 5' of the complete murine PDE4B3 coding sequence (NCBI NM_019840.2) and a hGH polyadenylation signal. AAV9-PDE4B was produced in AAV-293T cells (Stratagene #240073) with the three-plasmid method and calcium-chloride transfection. The virus was purified by cesium-chloride gradient. Viral particles titers were determined by RT-PCR on the CMV promoter. For control condition, an expression cassette encoding firefly luciferase under the control of a CMV promoter was packaged into AAV9 capsids and purified on cesium-chloride gradient to yield AAV9-Luc virus. AAV9-Luc or AAV9-PDE4B were injected *via* the tail vein at 10^{12} viral particles/mouse.

Transthoracic echocardiography

Transthoracic two-dimensional-guided M-mode echocardiography of mice was performed using an echocardiograph with a ML6 linear probe of 15 MHz (Vivid E9, General Electric Healthcare®) under 2% isoflurane gas and 0.8 L/min oxygen anaesthesia. Wall thickness and left ventricular chamber dimensions in systole and diastole were determined using parasternal short and long axes. Left ventricular mass (LVM) was calculated according to the Penn formula assuming a spherical LV geometry and validated for the mouse heart ($LVM=1.04\times[(LVIDd+IVS+PW)^3-(LVIDd)^3]$, where 1.04 is the specific gravity of muscle, LVIDd is left ventricular internal diameter in diastole, IVS and PW are end-diastolic

interventricular septum and posterior wall thicknesses. For the Transverse Aortic Constriction model (TAC), two days after the surgery, the severity of the constriction was evaluated by measuring the maximal flow velocity over the ligature with a 12S probe of 7.5 MHz using a continuous Doppler. Maximal pressure gradient (ΔP) was then calculated using the Bernouilli equation ($\Delta P=4Vmax^2$). Mice with maximal pressure gradients around 60 mmHg were included in the study. The average gradient was similar in the two groups (67.8±2.6 mmHg in mice injected with AAV-Luc *vs* 65,6±2.4 mmHg in mice injected with AAV-PDE4B). A blind analysis was performed for the echocardiographic images using EchoPac software (General Electric Healthcare®). Three measurements on three different sections were averaged for each of the two axes and for each of the measured parameters.

ECG and Telemetry

Six-lead surface electrocardiograms (ECG) were recorded in littermate pairs of 2 month-old mice during isoflurane inhalation (1-1.5 % plus oxygen). Recordings of 10 s were used for signal averaging. To record an ECG in freely roaming animals, telemetric ECG transmitters (model TA11PA-C10, Data Sciences International, St. Paul, MN, USA) were implanted under isoflurane anesthesia. The telemetric ECG was analyzed during normal activity over a 24-hour period one week after implantation. All recordings were digitized (EMKA, Falls Church, VA, USA) at 2 kHz and analyzed off-line.

Forced treadmill activity

Prior to the experiments, all mice were acclimatized to the rodent treadmill and running exercise by 6 min activity in the treadmill apparatus as follows:[3] Four days before the day of the experiment (D–4; running for 2 min at 10 $m.min^{-1}$, 4 min at 13 $m.min^{-1}$, 2 min at 15 $m.min^{-1}$, 2 min at 16.5 $m.min^{-1}$ and 2 min at 18 $m.min^{-1}$ at a 4% slope); 3 days before the day of the experiment (D–3; running for 2 min at 13 $m.min^{-1}$, 2 min at 16 $m.min^{-1}$, 2 min at 18 $m.min^{-1}$,

4 min at 20 $m.min^{-1}$ and 2 min at 22 $m.min^{-1}$ at a 4% slope). Compressed air, triggered by a photocell at the end of each lane, was used, if necessary, to maintain the running motivation during acclimatization and experiments. On the day of the experiment, to measure the maximal aerobic running performance, all animals were briefly warmed-up by running 10 $m.min^{-1}$ for 6 min. Then, animals were exercised until they were no longer able to maintain the increasing speed of the treadmill. Treadmill speed was increased by 3.3 $m.min^{-1}$ every 1.5 min to reach 30 $m.min^{-1}$ at a 4% slope, and then treadmill speed was increased by 3.3 $m.min^{-1}$ every min at a 4% slope. This allowed the maximal distance exercise ran capacity until exhaustion to be determined for each animal.

Perfused heart preparation

Male mice (PDE4B-TG and WT littermates) were anaesthetized with intraperitoneal injection of pentobarbital (150 mg/kg). The heart was quickly removed and placed into a solution for dissection containing (in mmol/L): NaCl 116, D-glucose 15, $NaHCO_3$ 25, KCl 4.7, KH_2PO_4 1.2, $MgSO_4$ 1.2, $CaCl_2$ 0.4, at 4°C, oxygenated (95% O_2–5% CO_2). Then, the aorta was cannulated and perfused by the Langendorff method with Krebs-Henseleit solution containing (in mmol/L): NaCl 116, D-glucose 11, $NaHCO_3$ 25, KCl 4.7, KH_2PO_4 1.2, $MgSO_4$ 1.2, $CaCl_2$ 1.2, Pyruvate 2, EDTA 0.1, at a constant pressure of 75 mm Hg and a temperature of 37.0±0.5°C. A latex balloon filled with water and ethanol (90/10) connected to a pressure transducer (Statham gauge Ohmeda, Bilthoven, The Netherlands) was introduced into the left ventricle after crossing the mitral valve. For each heart, the experiment started with a progressive increase of the latex balloon inserted inside the left ventricle to generate a ventricular volume-developed pressure relationship. When the maximal developed pressure was reached, ten minutes of equilibration in isovolumic working conditions were imposed before measuring cardiac parameters. Heart rate, left ventricular developed pressure (LVDP)

and the first derivatives of LV pressure (LV +dP/dtmax and LV -dP/dtmax) were measured online using a dedicated software (Emka technologies data analyzer, Paris, France). Then, the hearts were paced at 650 bpm using platinum electrode placed on the surface of the right ventricle and increasing concentrations of isoprenaline (Iso) were infused from 0.1 to 100 nmol/L. Pacing was stopped in the presence of 100 nmol/L Iso to record spontaneous cardiac parameters.

Isoprenaline infusion model

Male mice (WT or PDE4B-TG) at 10-weeks of age were treated for 14 days with either isoprenaline (60 mg/kg/day, Iso, Sigma) or vehicle (0.9% NaCl) administered via osmotic minipumps (2002, Alzet, USA) as described[4] with slight modifications. Two weeks after the end of the treatment, animal were anesthetized by intraperitoneal injection of pentothal (150 mg/kg). Hearts were rapidly removed and remaining blood was washed out in cold Ca^{2+}-free KREBS solution (120 mmol/L NaCl, 4.8 mmol/L KCl, 2.4 mmol/L $MgSO_4$-$7H_2O$, 1.2 mmol/L KH_2PO_4 and 24 mmol/L $NaHCO_3$). Transversal slice of 3-4 mm of width was cut in the middle of the heart and rapidly fixed in 10% formalin for histology. The rest of ventricular tissue was frozen in liquid nitrogen and stored at -80°C until use.

TAC model

Male C57/Bl6 mice aged 8 weeks were anesthetized by intraperitoneal injection of ketamine (100 mg/kg) and xylazine (10 mg/kg) and placed in a supine position atop a heating pad at 37°C. A 5 mm upper partial sternotomy was performed and the sternum retracted using a chest retractor. The thymus and fat tissue were gently separated from the aortic arch. Following identification of the transverse aorta, a small piece of a 4.0 silk suture was placed between the innominate and left carotid arteries. Two loose knots were tied around the transverse aorta and a small piece of 0.38 mm pin gauge was placed parallel to the transverse aorta. The first knot

was tied against the pin, followed by the second and the needle was promptly removed in order to yield a constriction of 0.38 mm in diameter. In sham control mice, the entire procedure is identical except for the ligation of the aorta. The sternum and the skin were closed using a 6.0 prolene suture with an interrupted suture pattern and the animal were then administered s.c. 0.03 μg/mg buprenorphine and allowed to recover on a heating pad until fully awake.

Histological and immunohistochemical analysis

Histological staining was performed as described previously. .Mouse hearts were fixed for 24 h in 10% formalin and then were paraffin embedded and transversely sectioned. Sections (3 μm) were deparaffinized and subjected to heat-induced epitope retrieval (HIER) in a 10 mmol/L citrate buffer. Cardiac fibrosis was assessed using Masson's trichrome stain kit (Microm France). To analyze apoptotic myocytes in the heart, autofluorescence was quenched by treating paraffin-embedded sections with PBS/BSA (5%) for 2 h before performing TUNEL staining (Roche) according to the manufacturer's protocol and using Proteinase K treatment. Sections were counterstained with Alexa Fluor 594-conjugated WGA (Invitrogen) at 10 μg/mL for 1 h at room temperature to visualize cell membranes. Slides were scanned by the digital slide scanner NanoZoomer 2.0-RS (Hamamatsu, Japan), which allowed an overall view of the samples. Images were digitally captured from the scan slides using the NDP.view2 software (Hamamatsu).

Preparation of mouse ventricular myocytes

Mice were anesthetized by intraperitoneal injection of pentothal (150 mg/kg), and the heart was quickly removed and placed into a cold Ca^{2+}-free Tyrode's solution containing 113 mmol/L NaCl, 4.7 mmol/L KCl, 1.2 mmol/L $MgSO_4$-$7H_2O$, 0.6 mmol/L KH_2PO_4, 0.6 mmol/L NaH_2PO_4, 1.6 mmol/L $NaHCO_3$, 10 mmol/L HEPES, 30 mmol/L Taurine, and 20 mmol/L glucose, adjusted to pH 7.4. The ascending aorta was cannulated, and the heart was perfused

with oxygenated Ca^{2+}-free Tyrode's solution at 37°C for 4 minutes using retrograde Langendorff perfusion. For enzymatic dissociation, the heart was perfused with Ca^{2+}-free Tyrode's solution containing LiberaseTM Research Grade (Roche Diagnostics) for 10 minutes at 37°C. Then the heart was removed and placed into a dish containing Tyrode's solution supplemented with 0.2 mmol/L $CaCl_2$ and 5 mg/ml BSA (Sigma-Aldrich). The ventricles were separated from the atria, cut into small pieces, and triturated with a pipette to disperse the myocytes. Ventricular myocytes were filtered on gauze and allowed to sediment by gravity for 10 minutes. The supernatant was removed, and cells were suspended in Tyrode's solution supplemented with 0.5 mmol/L $CaCl_2$ and 5 mg/ml BSA. Cells were suspended in Tyrode's solution with 1 mmol/L $CaCl_2$. For $I_{Ca,L}$ recording and Ionoptix experiments, freshly isolated ventricular myocytes were plated in 35-mm culture dishes coated with laminin (10 μg/ml) and stored at room temperature until use. For primary culture, Tyrode's solution was replaced by Minimum Essential Medium (MEM, 51200, Gibco) supplemented with 5% FBS, 2% penicillin-streptomycin, 0.1% BSA, 2 mmol/L L-glutamine, Insulin Transferin Selenium 1X and plated on 35 mm culture dishes coated with laminin (10 μg/ml) at a density of 10^4 cells per dish. AMVMs were left to adhere for 2 h in a 95% O_2, 5% CO_2 atmosphere at 37°C, before the medium was replaced with FBS-free MEM containing adenoviruses encoding the cAMP FRET sensor Epac-S^{H187} [5, 6] or the cytoplasmic PKA sensor AKAR3-NES[7, 8] at a multiplicity of infection of 1000 active viral particles per cell for 24 h.

Preparation of protein extracts

For PDE assay, frozen adult mouse hearts were homogenized in ice-cold buffer containing (in mmol/L): NaCl 150, HEPES 20 (pH 7.4), EDTA 2, and supplemented with 10% glycerol, 0.5% NP-40, 1 μmol/L microcystin-LR, and Complete Protease Inhibitor Tablets (Roche Diagnostics). Tissue lysates were centrifuged at 3,000 g and 4°C for 10 minutes, and

supernatants were used. For western blotting, frozen cardiac tissues were homogenized in a RIPA buffer containing (in mmol/L): NaCl (150, Tris-HCl 50 (pH 7.4), EDTA 2, and supplemented with 1% NP-40, 0.1% SDS, 1% Deoxycholate, Complete Protease Inhibitor Tablets and PhosSTOP^{TM} phosphatase inhibitor tablets (Roche Diagnostics). Tissue lysates were centrifuged at 15,000 g and 4°C for 20 minutes, and supernatants were used.

Real-time quantitative PCR

Total RNA was extracted from ventricular tissue using Trizol reagent (MRCgene). Reverse transcription of RNA samples was carried out by using iScript cDNA synthesis kit (Bio-Rad) according to manufacturer's instructions. Real-time PCR reactions were prepared using SYBR Green Supermix (Bio-Rad) and performed in a CFX96 TouchTM Real-Time PCR Detection System (Bio-Rad). The relative amount of mRNA transcripts was quantified using the ΔCt method. The average Ct obtained in non-treated cells was used as a calibrator and RPLP2 housekeeping gene was used as the reference for normalization. Sequences of the primers used are provided in Supplemental Table 2 below.

cAMP Assay

Basal cAMP levels in mouse hearts were measured with a cyclic AMP EIA kit (NewEast Biosciences) following the instructions from the manufacturer. Mouse ventricular tissue were first frozen and reduced to powder in liquid nitrogen. The tissue powder was weighted, diluted in 0.1 mol/L HCl, and used to detect the amount of cAMP.

PDE activity assay

Cyclic AMP-PDE activity was measured according to the method of Thompson and Appleman[9] as described previously.[10] In brief, samples were assayed in a 200 μL reaction mixture

containing 40 mmol/L Tris-HCl (pH 8.0), 1 mmol/L $MgCl_2$, 1.4 mmol/L β-mercaptoethanol, 1 μmol/L cAMP, 0.75 mg/ml bovine serum albumin, and 0.1 μCi of [^{3}H]cAMP for 15 minutes at 33°C. The reaction was terminated by heat inactivation in a boiling water bath for 1 minute. The PDE reaction product 5′-AMP was then hydrolyzed by incubation of the assay mixture with 50 μg Crotalus atrox snake venom for 20 minutes at 33°C, and the resulting adenosine was separated by anion exchange chromatography using 1 ml AG1-X8 resin (Bio-Rad) and quantified by scintillation counting.

Western blot analysis

Protein samples were separated in denaturating acrylamide gels and subsequently transferred onto PVDF membranes. After blocking the membranes with 5% milk buffer for 1 h, the incubation with primary antibodies was carried out over night at 4°C. After incubation with appropriate secondary antibodies for 1 h, proteins were visualized by enhanced chemoluminescence and quantified with Quantity One software. The primary antibodies used were: rabbit anti-PDE4B (113-4) raised against the C-terminus of PDE4B, rabbit anti-PDE4A (AC55), mouse anti-PDE4D (ICOS) (the three being kind gifts from Dr. Marco Conti, UCSF, California, USA), anti-phospholamban (PLB) (sc-21923, Santa Cruz), anti-p-PLB (Thr17) (A010-13, Badrilla), anti-p-PLB (Ser16) (A010-12, Badrilla), anti-troponin I (TnI) (4002, Cell Signaling), anti-p-TnI (Ser22-23) (4004, Cell Signaling), anti-myosin-binding protein C (MyBPC3) (sc-50115, Santa Cruz), anti-p-MyBPC3 (Ser282) (ALX-215-057-R050, Alexis), rabbit anti-PDE3A (a kind gift from Dr C. Yan, University of Rochester, Rochester, NY, USA), rabbit anti-PDE3B (University of Torino, Torino, Italy), mouse anti-β-actin (sc-47778, Santa Cruz), anti-calsequestrin (CSQ) (PA1-193, Pierce), mouse anti-vinculin (Vinc) (V9131, Sigma), rabbit anti-GAPDH (cell signalling).

$I_{Ca,L}$ current measurements

The whole-cell configuration of the patch-clamp technique was used to record $I_{Ca,L}$. Patch electrodes with 1–2 MΩ resistance when filled with internal solution contained 118 mmol/L CsCl, 5 mmol/L EGTA, 4 mmol/L $MgCl_2$, 5 mmol/L sodium phosphocreatine, 3.1 mmol/L Na_2ATP, 0.42 mmol/L Na_2GTP, 0.062 mmol/L $CaCl_2$ (pCa 8.5), and 10 mmol/L HEPES, adjusted to pH 7.3. External Cs^+-Ringer solution contained 107.1 mmol/L NaCl, 20 mmol/L CsCl, 4 mmol/L $NaHCO_3$, 0.8 mmol/L NaH_2PO_4, 5 mmol/L glucose, 5 mmol/L Na pyruvate, 10 mmol/L HEPES, 1.8 mmol/L $MgCl_2$, and 1.8 mmol/L $CaCl_2$, adjusted to pH 7.4. The cells were depolarized every 8 seconds from –50 mV to 0 mV for 400 ms. The use of –50 mV as holding potential allowed the inactivation of voltage-dependent sodium currents. Potassium currents were blocked by replacing all K^+ ions with external and internal Cs^+.

Measurements of Ca^{2+} transients and cell shortening

Isolated cardiomyocytes were loaded with 3 μM Fura-2 AM (Invitrogen) at room temperature for 15 minutes and then washed with external Ringer solution containing (in mmol/L): NaCl 121.6, KCl 5.4, $NaHCO_3$ 4.013, NaH_2PO_4 0.8, 10 mM HEPES, glucose 5, Na pyruvate 5, $MgCl_2$ 1.8, and $CaCl_2$ 1, pH 7.4. The loaded cells were field stimulated (5 V, 4 ms) at a frequency of 0.5 Hz. Sarcomere length (SL) and Fura-2 ratio (measured at 512 nm upon excitation at 340 nm and 380 nm) were simultaneously recorded using an IonOptix System (IonOptix®). Cell contractility was assessed by the percentage of sarcomere shortening, which is the ratio of twitch amplitude (difference of end-diastolic and peak systolic SL) to end-diastolic SL. Ca^{2+} transients were assessed by the percentage of variation of the Fura-2 ratio by dividing the twitch amplitude (difference of end-diastolic and peak systolic ratios) to end-diastolic ratio. The Tau was used as an index of relaxation and Ca^{2+} transient decay kinetics. All parameters were calculated offline using a dedicated software (IonWizard 6x).

Cyclic AMP level and PKA activity measurements by fluorescent resonance energy transfer (FRET) imaging

Freshly isolated ventricular myocytes from PDE4B-TG and WT mice were infected with adenoviruses to measure cAMP and PKA activity, respectively. The cells were then washed once and maintained in the Ringer solution described above containing 1.8 mmol/L $CaCl_2$, at room temperature, Images were captured every 5 seconds using the 40× oil immersion objective of an inverted microscope (Nikon) connected to a software-controlled (Metafluor, Molecular Devices) cooled charge coupled (CCD) camera (Cool SNAP HQ2). CFP was excited during 300 ms by a Xenon lamp (100W, Nikon) using a 440/20BP filter and a 455LP dichroic mirror. Dual emission imaging of CFP and YFP was performed using a Dual-View emission splitter equipped with a 510LP dichroic mirror and 480/30 nm, 535/25 nm BP filters. Average fluorescence intensity was measured in a region of interest comprising the entire cell. Background was subtracted and CFP bleed through in the YFP channel was corrected before calculating the YFP/CFP ratio for the AKAR3-NES sensor or the CFP/YFP ratio for the Epac-S^{H187} sensor. Ratio images were obtained using Image J software.

Statistics

All results are expressed as mean±SEM and were analyzed using the GraphPad Prism software (GraphPad software, Inc., La Jolla, CA, USA). Normal distribution was tested by the Shapiro-Wilk normality test. For simple two-group comparison, we used an unpaired Student t-test or a Mann-Whitney test when the data did not follow a normal distribution. Differences between multiple groups were analyzed using an ordinary one-way ANOVA with Tukey's multiple comparisons post-hoc test, or a Kruskal Wallis with Dunn's multiple comparisons post-hoc test, when the data did not follow a normal distribution. Two-way ANOVA (ordinary or mixed-effects) with Sidak's or Tukey's post-hoc test was used when appropriate. P-value<0.05 was considered statistically significant.

References

1. Cherry JA, Thompson BE and Pho V. Diazepam and rolipram differentially inhibit cyclic AMP-specific phosphodiesterases PDE4A1 and PDE4B3 in the mouse. *Biochim Biophys Acta*. 2001;1518:27-35.
2. Gulick J, Subramaniam A, Neumann J and Robbins J. Isolation and characterization of the mouse cardiac myosin heavy chain genes. *J Biol Chem*. 1991;266:9180-5.
3. Habouzit E, Richard H, Sanchez H, Koulmann N, Serrurier B, Monnet R, Ventura-Clapier R and Bigard X. Decreased muscle ACE activity enhances functional response to endurance training in rats, without change in muscle oxidative capacity or contractile phenotype. *J Appl Physiol (1985)*. 2009;107:346-53.
4. Irie T, Sips PY, Kai S, Kida K, Ikeda K, Hirai S, Moazzami K, Jiramongkolchai P, Bloch DB, Doulias PT, Armoundas AA, Kaneki M, Ischiropoulos H, Kranias E, Bloch KD, Stamler JS and Ichinose F. S-Nitrosylation of Calcium-Handling Proteins in Cardiac Adrenergic Signaling and Hypertrophy. *Circ Res*. 2015;117:793-803.
5. Klarenbeek J, Goedhart J, van Batenburg A, Groenewald D and Jalink K. Fourth-Generation Epac-Based FRET Sensors for cAMP Feature Exceptional Brightness, Photostability and Dynamic Range: Characterization of Dedicated Sensors for FLIM, for Ratiometry and with High Affinity. *PLoS One*. 2015;10:e0122513.
6. Vettel C, Lindner M, Dewenter M, Lorenz K, Schanbacher C, Riedel M, Lammle S, Meinecke S, Mason FE, Sossalla S, Geerts A, Hoffmann M, Wunder F, Brunner FJ, Wieland T, Mehel H, Karam S, Lechene P, Leroy J, Vandecasteele G, Wagner M, Fischmeister R and El-Armouche A. Phosphodiesterase 2 Protects Against Catecholamine-Induced Arrhythmia and Preserves Contractile Function After Myocardial Infarction. *Circ Res*. 2017;120:120-132.
7. Allen MD and Zhang J. Subcellular dynamics of protein kinase A activity visualized by FRET-based reporters. *Biochem Biophys Res Commun*. 2006;348:716-21.
8. Haj Slimane Z, Bedioune I, Lechene P, Varin A, Lefebvre F, Mateo P, Domergue-Dupont V, Dewenter M, Richter W, Conti M, El-Armouche A, Zhang J, Fischmeister R and Vandecasteele G. Control of cytoplasmic and nuclear protein kinase A by phosphodiesterases and phosphatases in cardiac myocytes. *Cardiovasc Res*. 2014;102:97-106.
9. Thompson WJ and Appleman MM. Multiple cyclic nucleotide phosphodiesterase activities from rat brain. *Biochemistry*. 1971;10:311-6.
10. Abi-Gerges A, Richter W, Lefebvre F, Mateo P, Varin A, Heymes C, Samuel JL, Lugnier C, Conti M, Fischmeister R and Vandecasteele G. Decreased expression and activity of cAMP phosphodiesterases in cardiac hypertrophy and its impact on beta-adrenergic cAMP signals. *Circ Res*. 2009;105:784-92.

Supplemental Table 1

Morphometric and echocardiographic parameters

WT and PDE4B-TG mice (line A) at 10 weeks of age

	WT			PDE4B-TG		
	Mean	**sem**	**N**	**Mean**	**sem**	**N**
Morphometric analysis						
HW (mg)	170	7	14	202**	7	19
LW (mg)	150	6	14	154	4	19
BW (g)	28.1	0.7	14	29.5	0.5	19
TL (mm)	18.2	0.1	14	18.2	0.1	19
HW/BW (mg/g)	6.0	0.2	14	6.9**	0.2	19
LW/BW (mg/g)	5.3	0.1	14	5.2	0.1	19
Echocardiography						
EF (%)	68.4	2.4	21	51.4***	2.4	26
LVIDd (mm)	3.9	0.1	21	4.2	0.1	26
IVSd (mm)	0.72	0.02	21	0.72	0.02	26
PWd (mm)	0.72	0.02	21	0.75	0.02	26
LVIDs (mm)	2.6	0.1	21	3.24***	0.11	26
IVSs (mm)	1.05	0.04	21	0.96	0.02	26
PWs (mm)	0.98	0.02	21	0.96	0.02	26

Student t test. **p<0,01, ***p<0,001.

HW, heart weight; LW, lung weight; BW, body weight, TL, tibia length; EF, ejection fraction; LVIDd, end-diastolic left ventricular internal diameter; IVSd, end-diastolic interventricular septum; PWd, end-diastolic posterior wall; LVIDs, end-systolic left ventricular internal diameter; IVSs, end-systolic interventricular septum; PWs, end-systolic posterior wall.

Supplemental Table 2

Sequences of the primers used in qRT-PCR experiments

Gene	Orientation	Primer sequence 5' – 3'	Species
Nppa	Forward	AGGCCATATTGGAGCAAATC	rat, mouse
	Reverse	CTCCTCCAGGTGGTCTAGCA	
Nppb	Forward	CTGGGAAGTCCTAGCCAGTC	rat, mouse
	Reverse	TTTTCTCTTATCAGCTCCAGCA	
Myh7	Forward	ATGTGCCGGACCTTGGAAG	mouse
	Reverse	CCTCGGGTTAGCTGAGAGATCA	
Rcan1	Forward	CAGCGAAAGTGAGACCAGGG	mouse
	Reverse	ACGGGGGTGGCATCTTCTAC	
Pde4b	Forward	ACGGTGGCTCATACATGCT	mouse
	Reverse	GTACCAGTCCCGACGAAGAG	

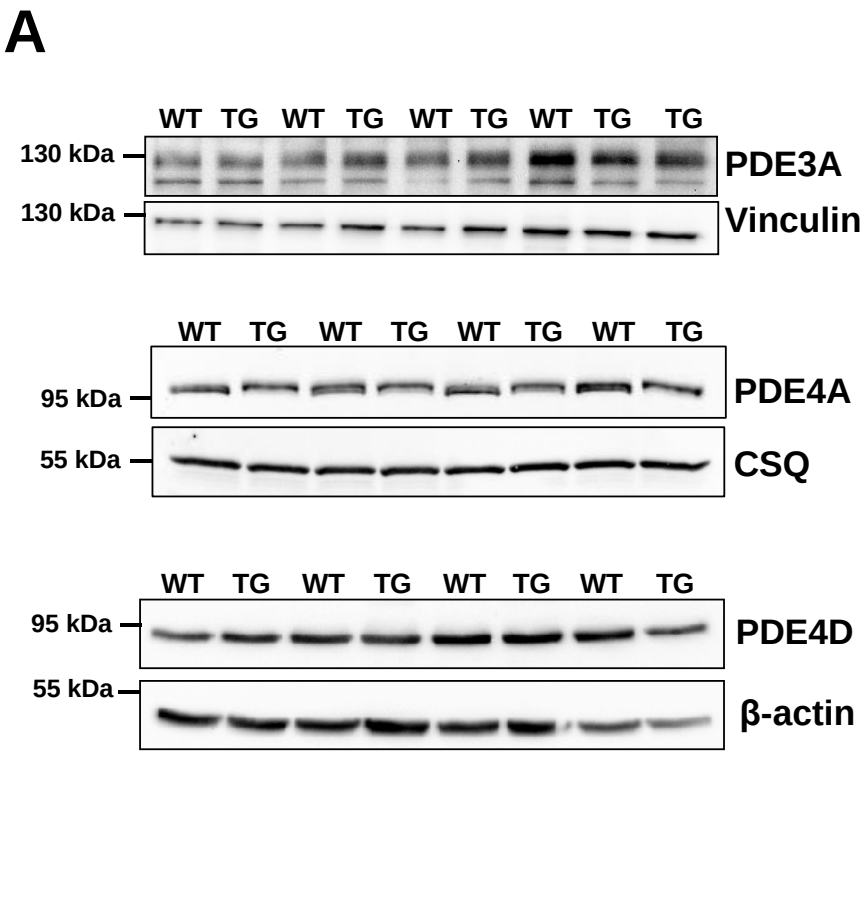

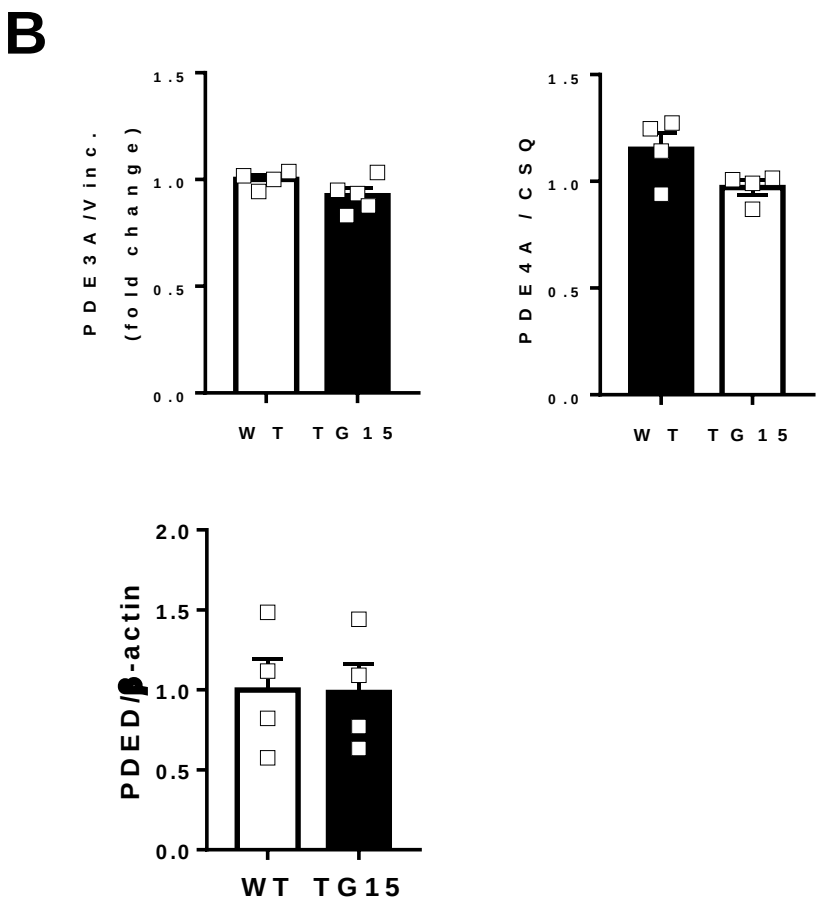

Supplemental Figure 1

Supplemental Figure 1: Expression of the main cardiac PDE isoforms other than PDE4B in TG15 hearts. A, Representative western blots of PDE3A, PDE4A, and PDE4D isoforms in cardiac tissue lysates from WT and TG15 mice. B, Quantification of data obtained in several immunoblots from at least 4 WT and 4 TG15. Vinculin and β-actin were used as loading controls. Bars represent the mean ± SEM. Mann-Whitney test (B).

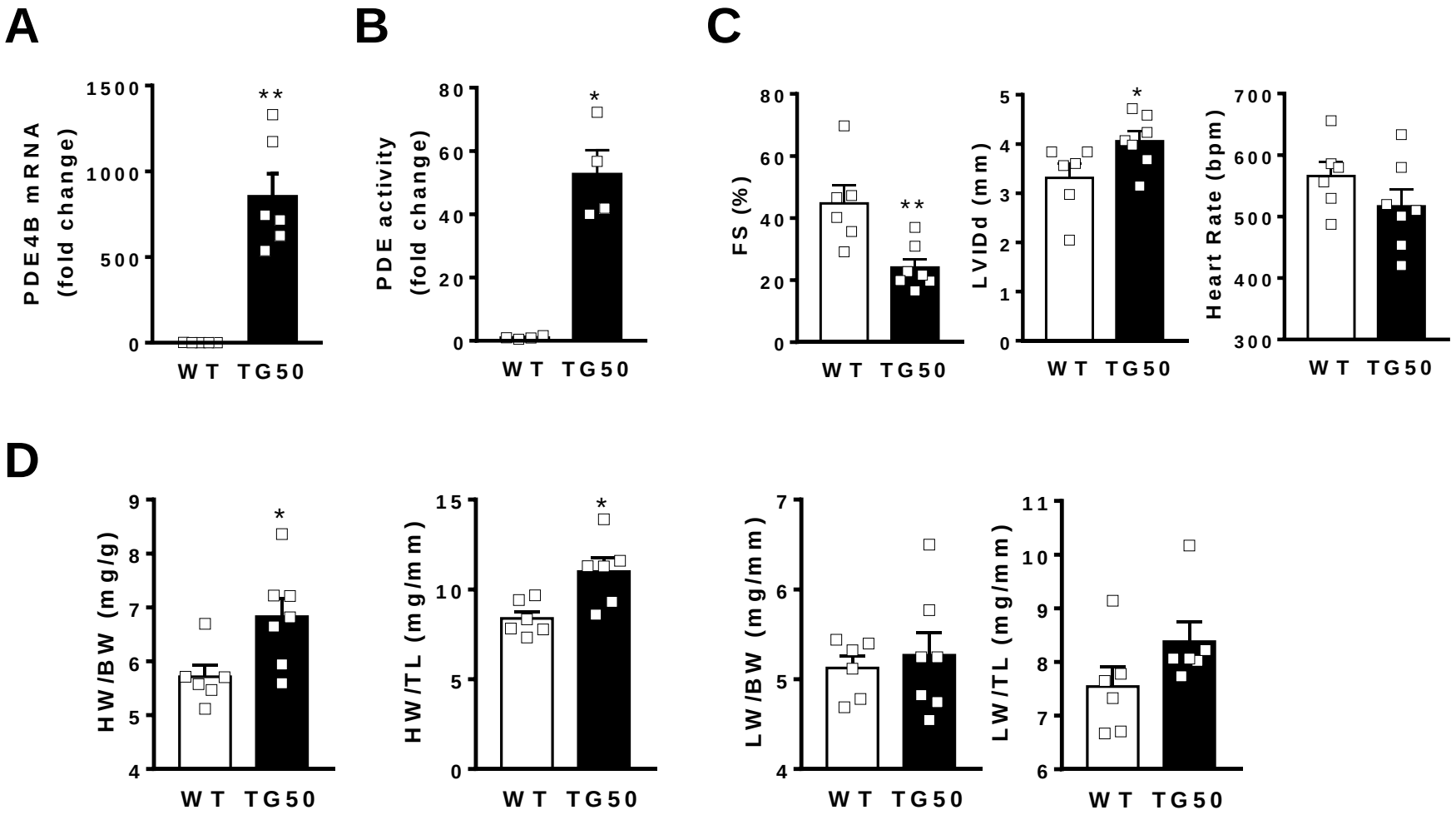

Supplemental Figure 2

Supplemental Figure 2: Characterization of PDE4B-TG mouse line TG50 at 10-12 weeks of age. A, PDE4B mRNA expression in WT (N=5) and TG50 (N=6) hearts measured by qRT-PCR. B, Total cAMP-PDE in heart extracts from WT (N=4) and TG50 (N=4) mice measured by radioenzymatic assay with 1 µM cAMP as a substrate. C, Heart rate, fractional shortening (FS), and end-diastolic left ventricular internal diameter (LVIDd) evaluated by echocardiography in anesthetized WT (N=6) and TG50 (N=7) mice. D, Heart weight (HW) and lung weight (LW) normalized to body weight (BW) or to tibia length (TL) in WT and TG50 mice (N=6/7 per group). Bars represent the mean ± SEM. **P*<0.05; ***P*<0.01, Mann-Whitney test.

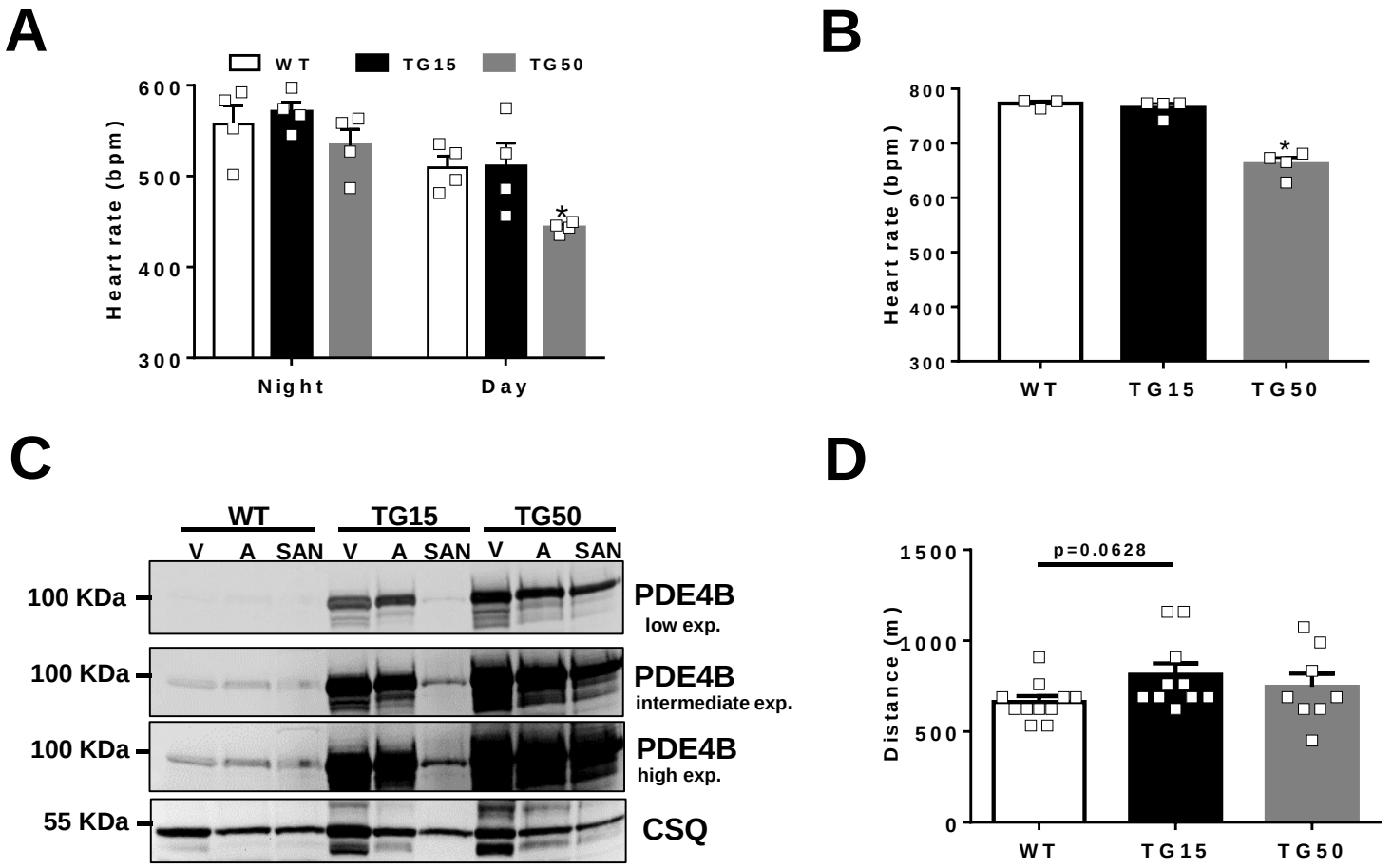

Supplemental Figure 3

Supplemental Figure 3: Heart rate regulation and exercise capacity in WT and PDE4B-TG mouse lines (TG15 and TG50). A, Average heart rate during night and day measured by telemetry (N=4 per group). B, Heart rate measured in WT (N=3), TG15 (N=4) and TG50 mice (N=4) by telemetry during exercise on a treadmill at a speed of 2 km/h. C, Western blot analysis of PDE4B expression in left ventricle (V), left atria (A) and sino-atrial node (SAN) from WT, TG15 and TG50. Calsequestrin (CSQ) was used as a loading control. Shown are low, intermediate and high exposures of one representative blot of 5 similar independent experiments. D, Average distance run on a treadmill exercise to exhaustion in WT (N=11), TG15 (N=10), and TG50 (N=8). *P<0.05, Two-way repeated measures ANOVA with Sidak's multiple comparison test (A); Kruskal-Wallis test followed by Dunn's multiple comparisons test (B, D).

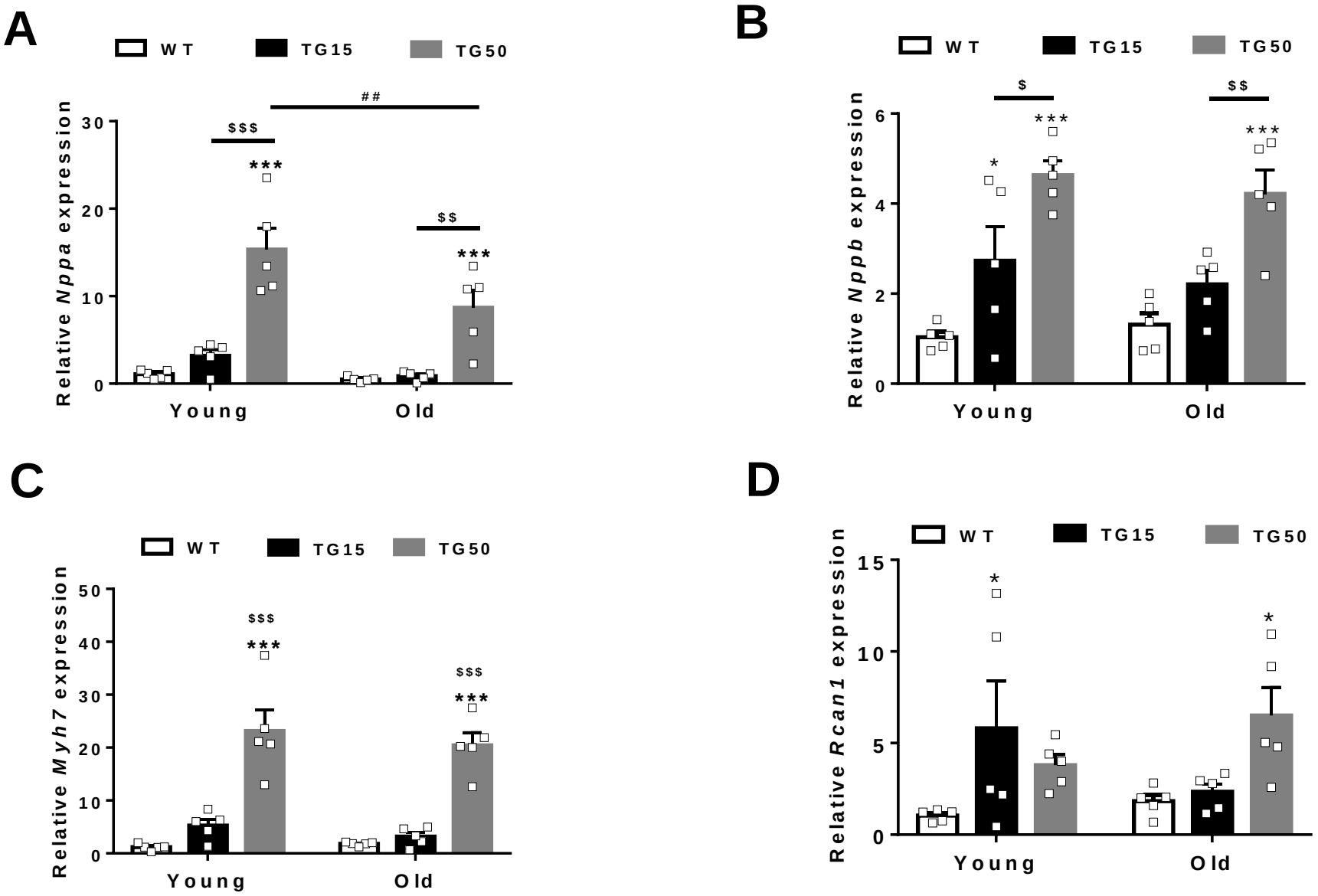

Supplemental Figure 4

Supplemental Figure 4: Comparative expression of hypertrophic marker genes in young (10-15 weeks) and old (58-60 weeks) WT, TG15 and TG50 lines. Expression of the atrial natriuretic peptide gene, *Nppa* (A), of the brain natriuretic peptide gene, *Nppb* (B), of the β isoform of the myosin heavy chain gene, *Myh7* (C) and of the regulator of calcineurin 1 gene, *Rcan1* (D) determined by qRT-PCR in total RNA extracted from the left ventricle of young and old WT, TG15 and TG50 mice (N=5 mice per group). Two-way ANOVA with Sidak's multiple comparisons test. Statistical significance between TG15 and WT or between TG50 and WT is indicated by $*P<0.05$, $***P<0.001$; between TG15 and TG50 by $^{\$}P<0.05$, $^{\$\$}P<0.01$, $^{\$\$\$}P<0.001$ and between Young and Old by $^{\#\#}P<0.01$.

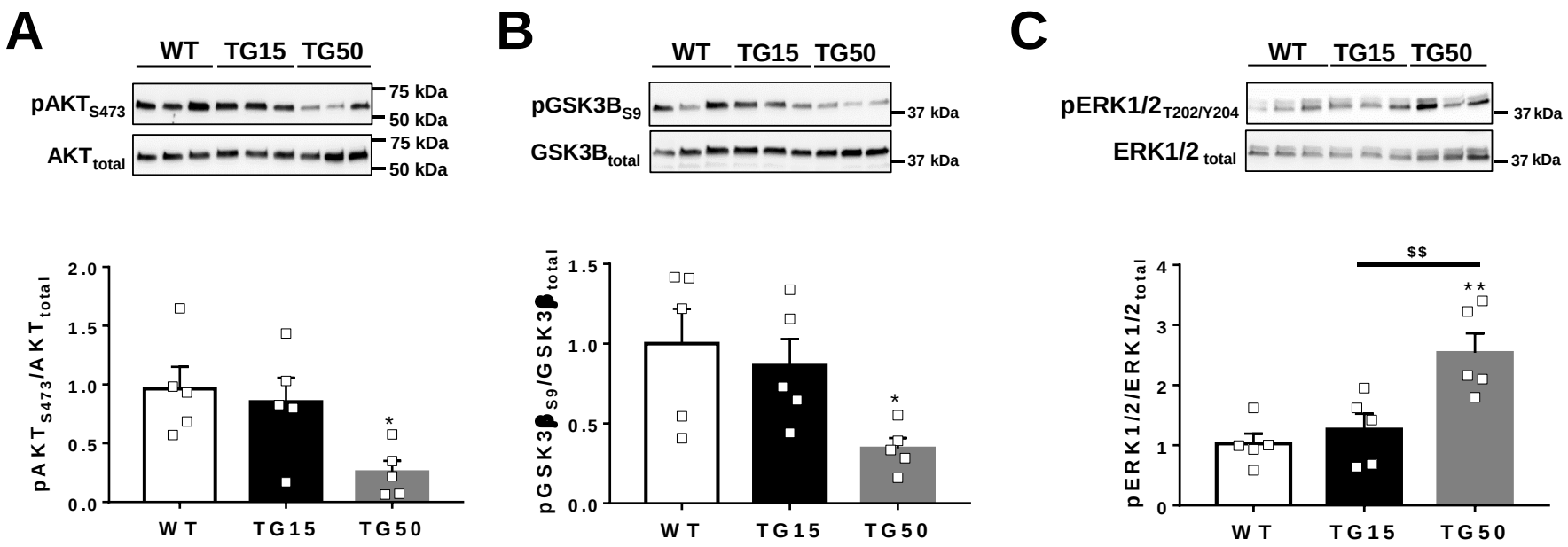

Supplemental Figure 5

Supplemental Figure 5: Modification of AKT/GSK3β and ERK1/2 pathways in hearts from TG50 mice but not from TG15 mice. Western blot analysis of AKT phosphorylation at Ser473 (A), GSK3β at Ser9 (B), and ERK1/2 at T202 and Y204 (C) in young (10-15 weeks) WT (N=5), TG15 (N=5) and TG50 (N=5) mice. Statistical significance is indicated as **P*<0.05, ***P*<0.01 between TG50 and WT; $^{\$\$}$*P*<0.01 between TG15 and TG50; one-way ANOVA, Holm-Sidak's multiple comparison test.

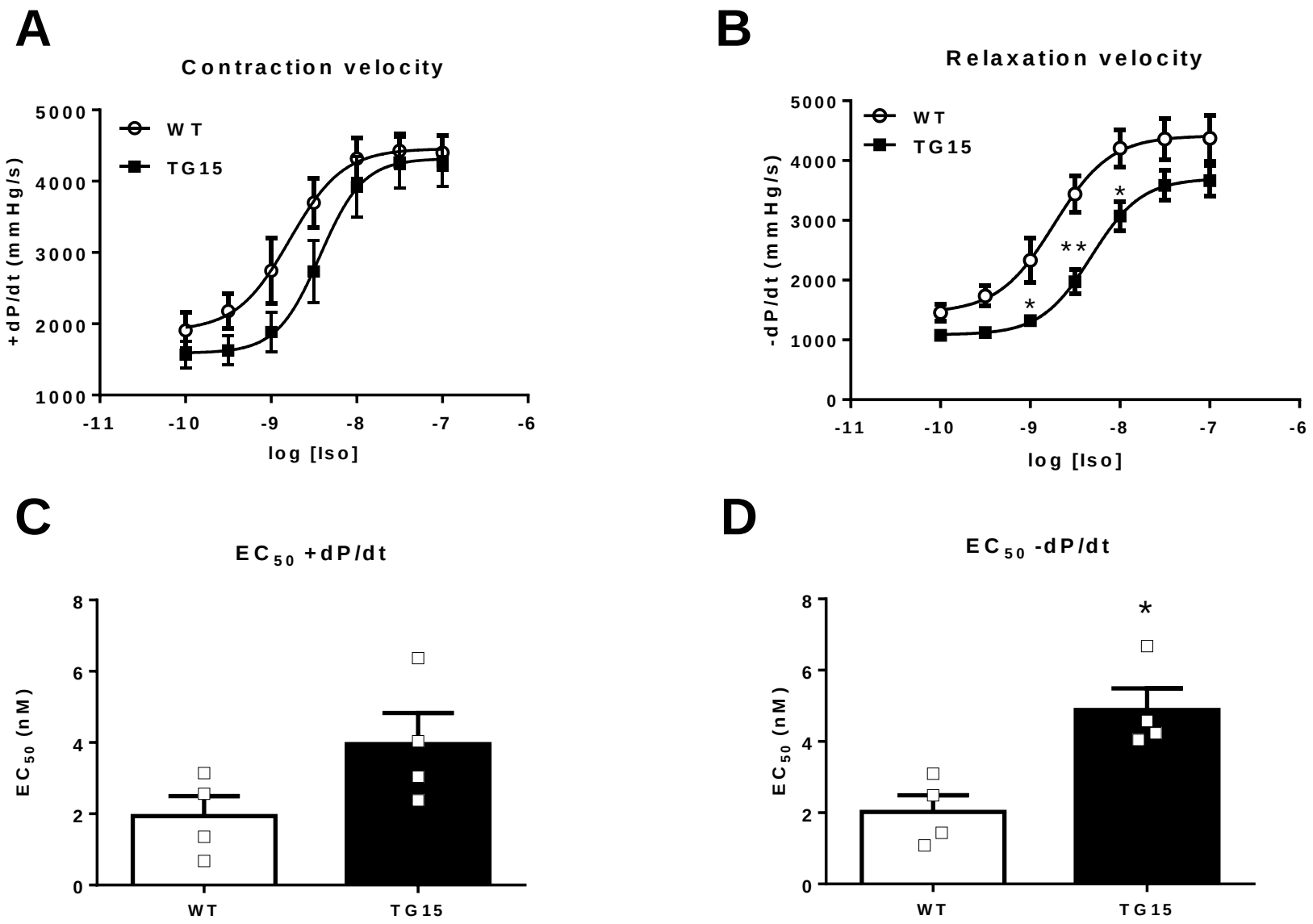

Supplemental Figure 6

Supplemental Figure 6: Decreased potency of isoprenaline on the inotropic and lusitropic response in isolated, perfused hearts from TG15 mice. A, B, Concentration-response curves to isoprenaline (Iso) on contraction and relaxation kinetics in WT and PDE4B-TG hearts paced at 650 bpm (N=4 in each group). C, D, EC_{50} values deduced from the curves obtained in A and B, respectively. *P<0.05, Mann-Whitney test.

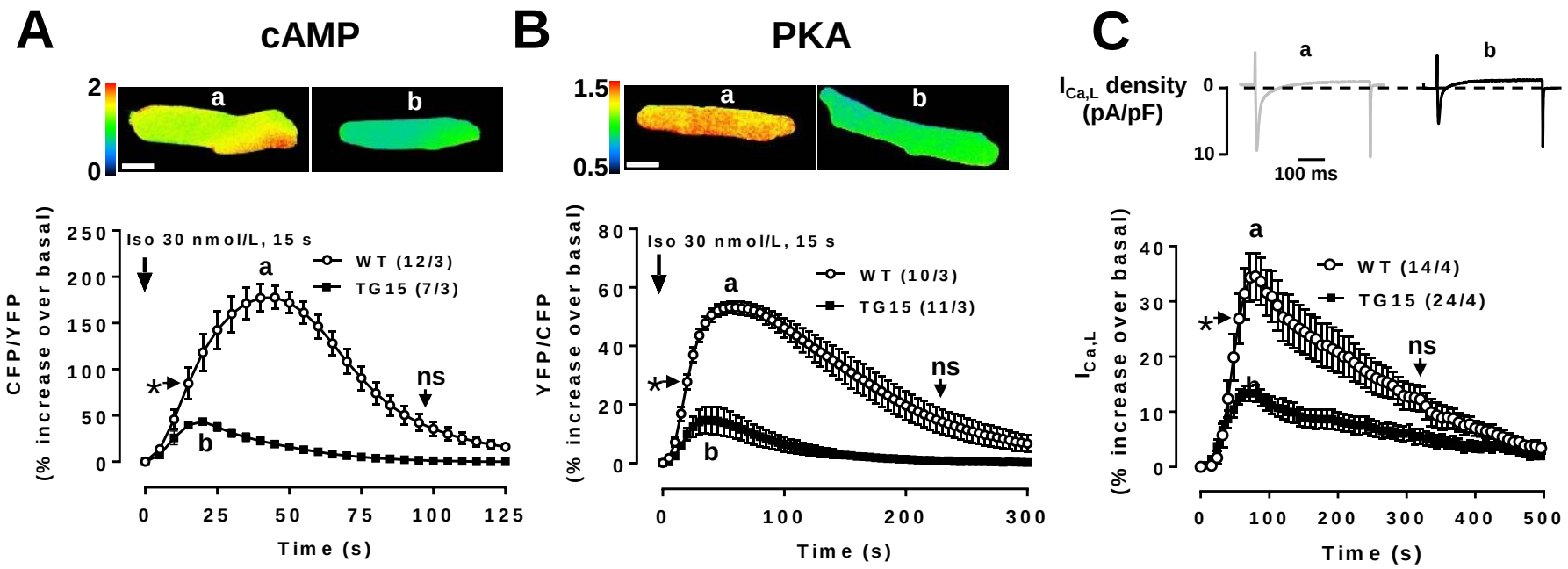

Supplemental Figure 7

Supplemental Figure 7: Blunted β-AR stimulation of cAMP, PKA and L-type Ca^{2+} current in ventricular myocytes from TG15 mice. A, B, Normalized average time course of the CFP/YFP ratio and the YFP/CFP ratio used as index of intracellular [cAMP] and PKA activity, respectively, in response to a 15 s application of Iso (30 nmol/L) in wild-type (WT) and TG15 ventricular myocytes expressing the FRET-based cAMP sensor EPAC-S^{H187} (A) or the FRET-based PKA activity reporter, AKAR3-NES (B). Numbers in brackets indicate number of cells and mice. Representative pseudocolor images of the FRET ratio recorded at the time indicated by the letters on the graphs for WT and TG15 are shown. ns, not significant. C, Mean variation of $I_{Ca,L}$ amplitude following Iso application (30 nmol/L, 15 s). The individual current traces shown on top were recorded at the times indicated by the corresponding letters in the graph below. **P*<0.05, ***P*<0.01, ****P*<0.001, Two-way repeated measures ANOVA with Tukey's multiple comparison test (A-C).

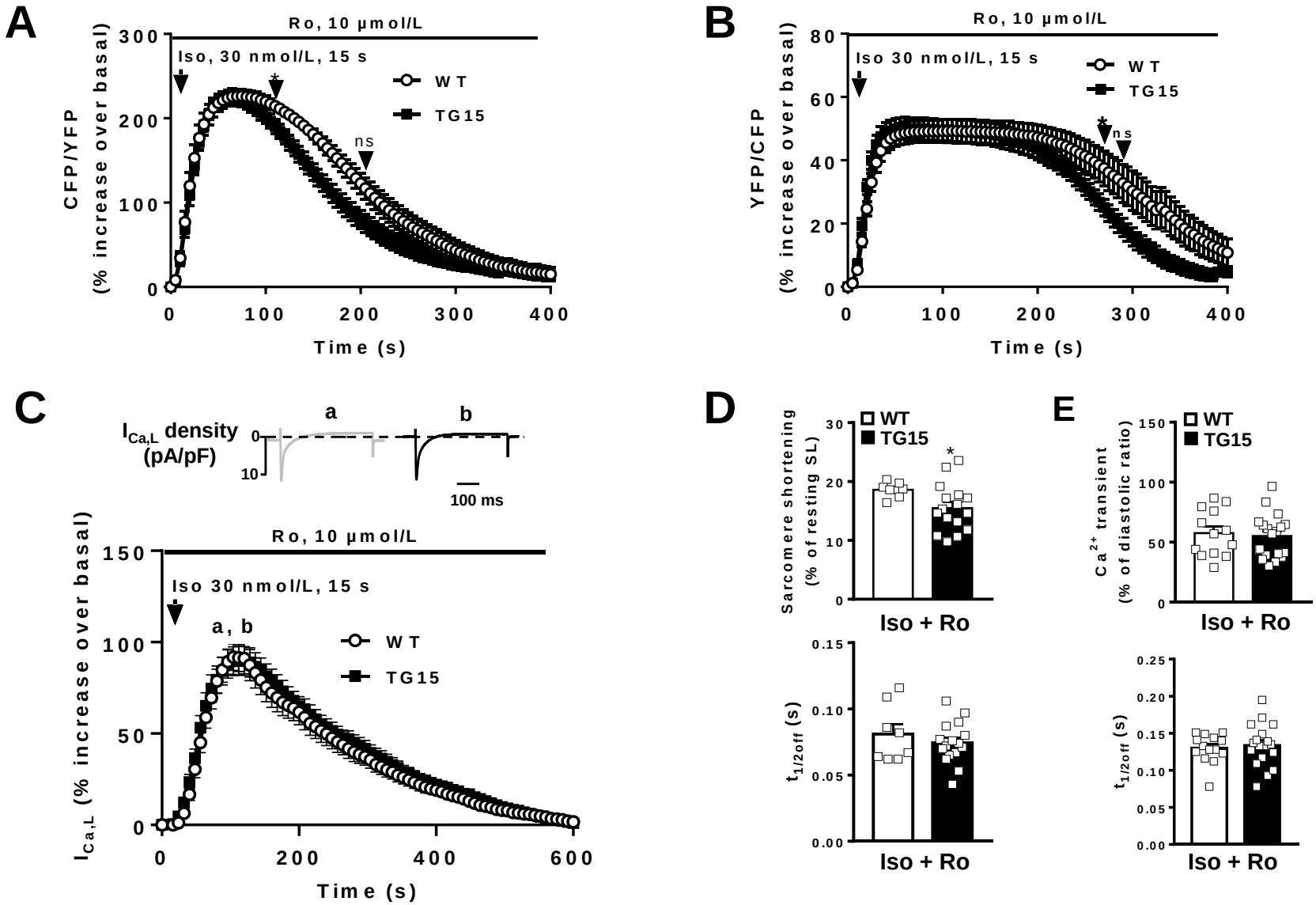

Supplemental Figure 8

Supplemental Figure 8: PDE4 inhibition normalizes β-AR responses in TG15 cardiomyocytes. A-C, Isolated ventricular myocytes from WT and TG15 mice were pre-incubated with Ro20-1724 (Ro, 10 µmol/L) prior to pulse stimulation with isoprenaline (Iso, 30 nmol/L) and the PDE4 inhibitor was maintained throughout the rest of the experiments. A, Mean variation of intracellular cAMP levels measured with EPAC-S^{H187} in WT (N=3, n=12) and TG15 myocytes (N=3, n=7). B, Mean variation of PKA activity measured with AKAR3-NES after in WT (N=3, n=8) and TG15 myocytes (N=3, n=7). C, Mean variation of $I_{Ca,L}$ in WT (N=4, n=13) and TG15 (N=4, n=25). Individual traces of $I_{Ca,L}$ at the time indicated by the letters on the graph are presented. D, Mean sarcomere shortening and relaxation kinetics ($t_{1/2}$ values) of cardiomyocytes from WT (N=7, n=8) and TG15 mice (N=6, n=16) in the presence of Iso (100 nmol/L) and Ro (10 µmol/L). E, Mean amplitude of Ca^{2+} transient and relaxation kinetics ($t_{1/2}$ values from WT (N=6, n=13) and TG15 mice (N=6, n=18). Graphs represent the mean ± SEM. **P*<0.05, Two-way repeated measures ANOVA with Tukey's multiple comparison test (A-C) ; Student t-test (D,E).

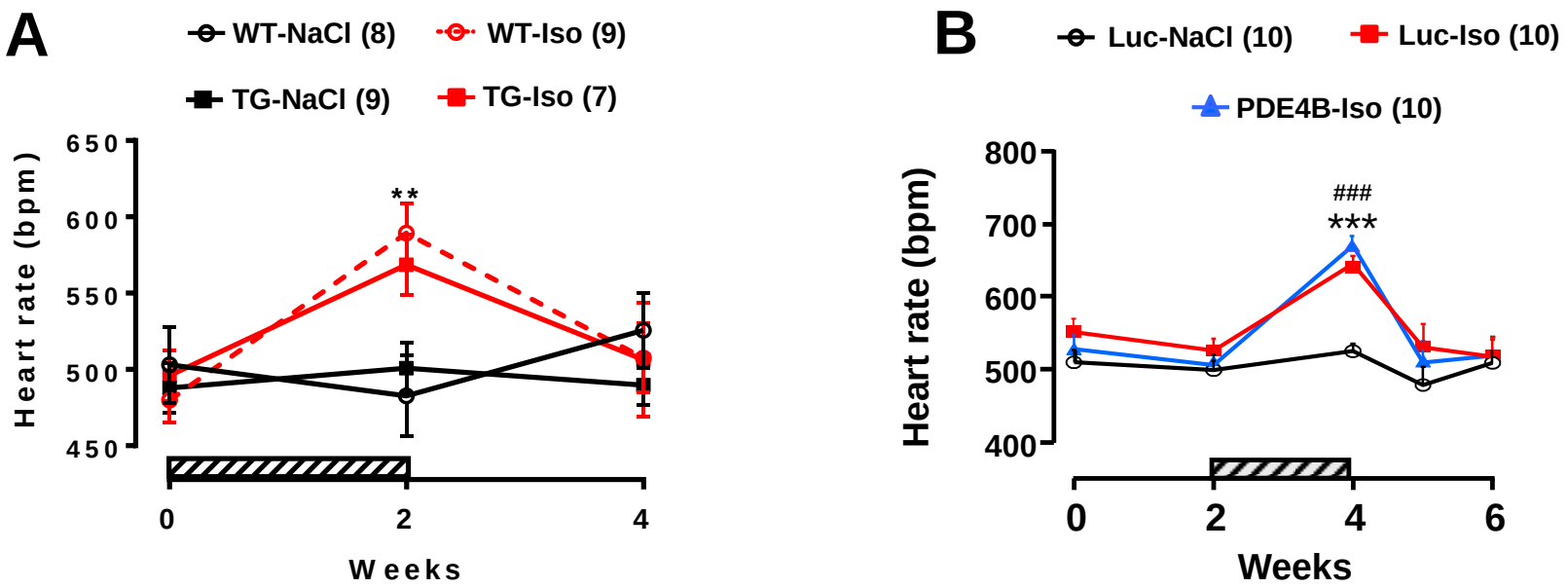

Supplemental Figure 9

Supplemental Figure 9: Effectiveness of Iso diffusion *via* osmotic minipumps is attested by increased heart rate measured by echocardiography. A, Mean heart rate measured before, at 2 weeks and at 4 weeks after minipump implantation in WT and TG15 mice. Minipumps delivered 60 mg/kg/day of Iso or 0.9% NaCl during the period indicated by the hatched bar. WT Iso *vs* WT NaCl: $^{**}P<0.01$. Two-way, mixed-effects ANOVA with Tukey's multiple comparison test. B, Time course of mean heart rate measured in mice injected with AAV9-Luc or AAV9-PDE4B and treated with 60 mg/kg/day Iso or NaCl during the period indicated by the hatched bar. Iso-Luc or Iso-PDE4B *vs* NaCl-Luc: $^{***}P<0.001$, $^{###}P<0.001$. Two-way, mixed-effects ANOVA with Tukey's multiple comparison test.

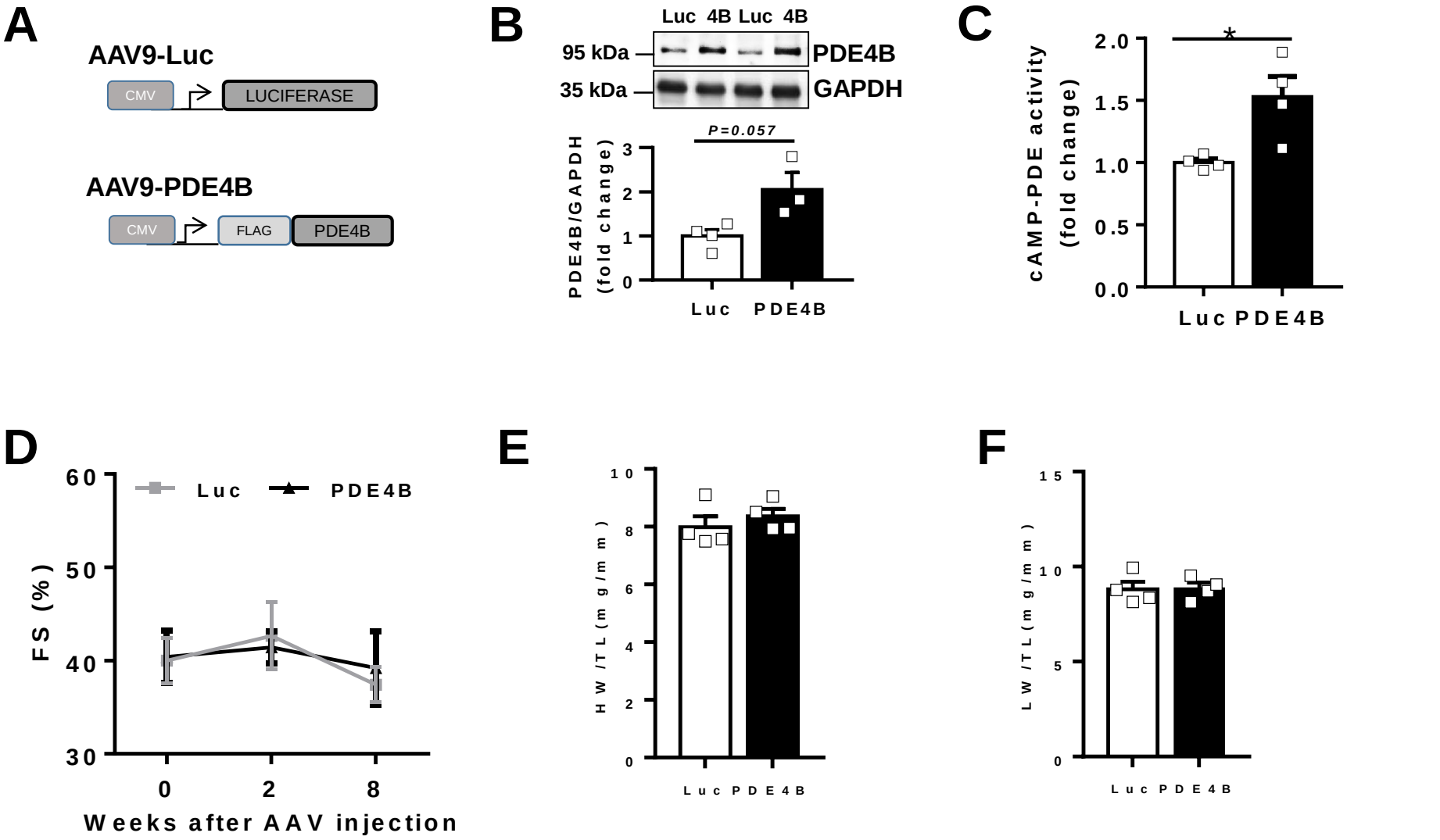

Supplemental Figure 10

Supplemental Figure 10: PDE4B overexpression by AAV9 does not affect physiological heart function. A, Schematic representation of the constructions used to produce the viruses. Both viruses express the protein of interest downstream of cytomegalovirus promoter (CMV). AAV9-Luc expresses the Luciferase (Luc) protein and is used as a control, AAV9-PDE4B (4B) expresses the longest isoform of PDE4B (NM_019840.2) fused with a FLAG-tag (MDYKDDDDK) at the N-terminal. B, PDE4B protein expression in heart extracts measured by Western blot (AAV9-Luc: N=4; AAV9-PDE4B: N=3). C, Total cAMP-PDE measured in mice ventricular protein extracts (N=4 per group). D, Time course analysis of fractional shortening measured by echography in mice. (N=4 per group). E, F Quantification of heart weight (HW, E) and lung weight (LW, F), over tibia length (TL) ratios (N=4 per group). *P<0.05, Mann-Whitney test (B,C), Two-way, mixed-effects ANOVA (D); Mann-Whitney test (E, F).

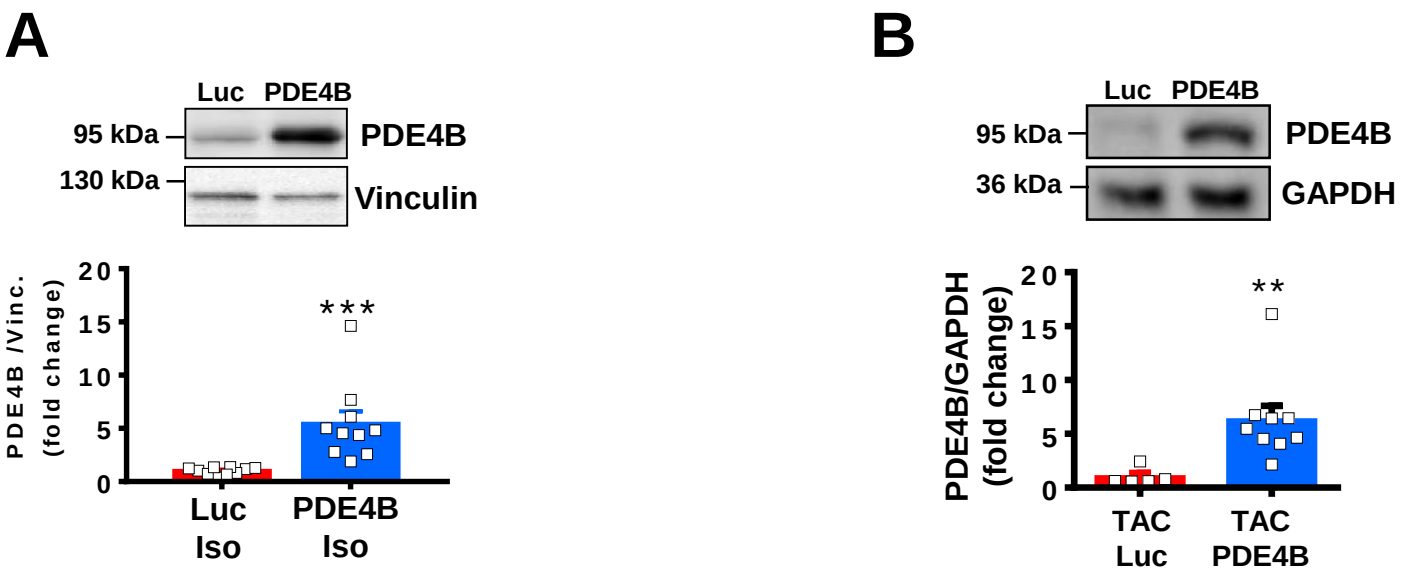

Supplemental Figure 11

Supplemental Figure 11: Assessment of cardiac PDE4B expression following AAV9 injection in mice treated with chronic Isoprenaline (Iso) and subjected to trans-aortic constriction (TAC). A, Western blot analysis of PDE4B protein in heart extracts from mice injected with 10^{12} AAV9-Luc or AAV9-PDE4B and treated with Iso (60 mg/kg/day) during two weeks. Number of mice is indicated inside the bars (same animals as in Fig. 7). B, Western blot analysis of PDE4B protein in heart extracts from mice subjected to TAC and injected with 10^{12} AAV9-Luc or AAV9-PDE4B. Number of mice is indicated inside the bars (same animals as in Fig. 8). ***P<0.01*, ****P*<0.001, Mann-Whitney test.

Original gel images of western blot analysis

Red dotted boxes indicate the part of the blot that is included in the manuscript figures.

Figure 1A

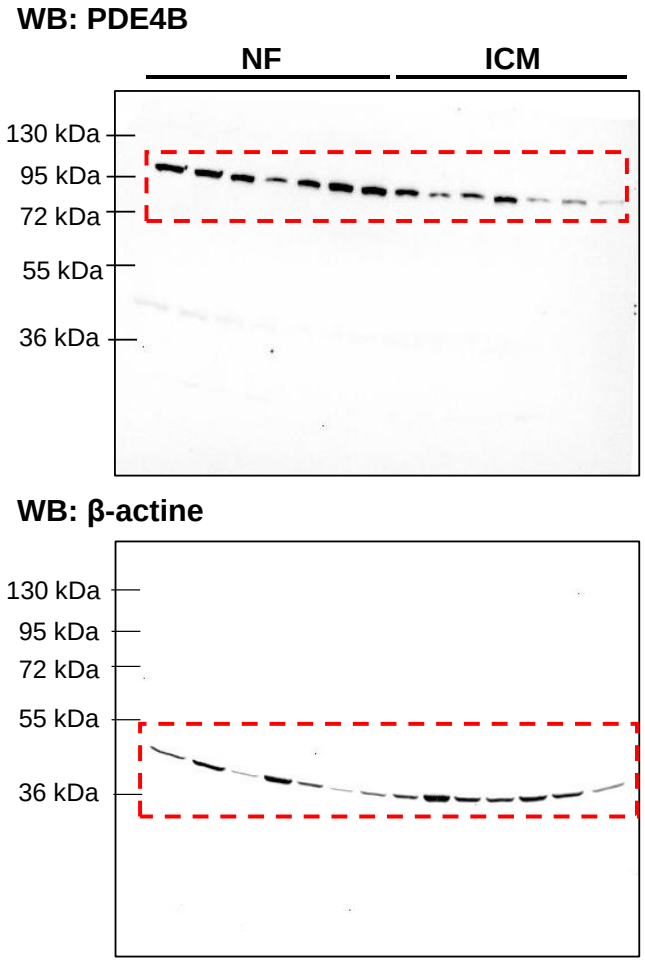

Figure 1B

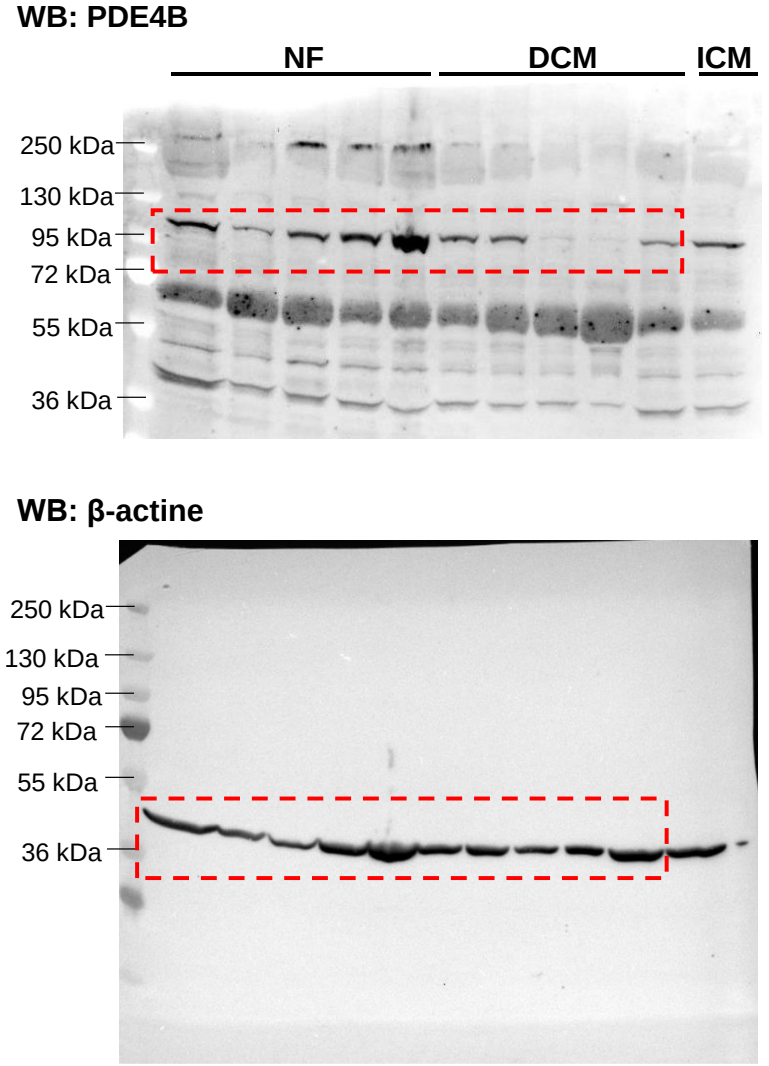

Figure 2B

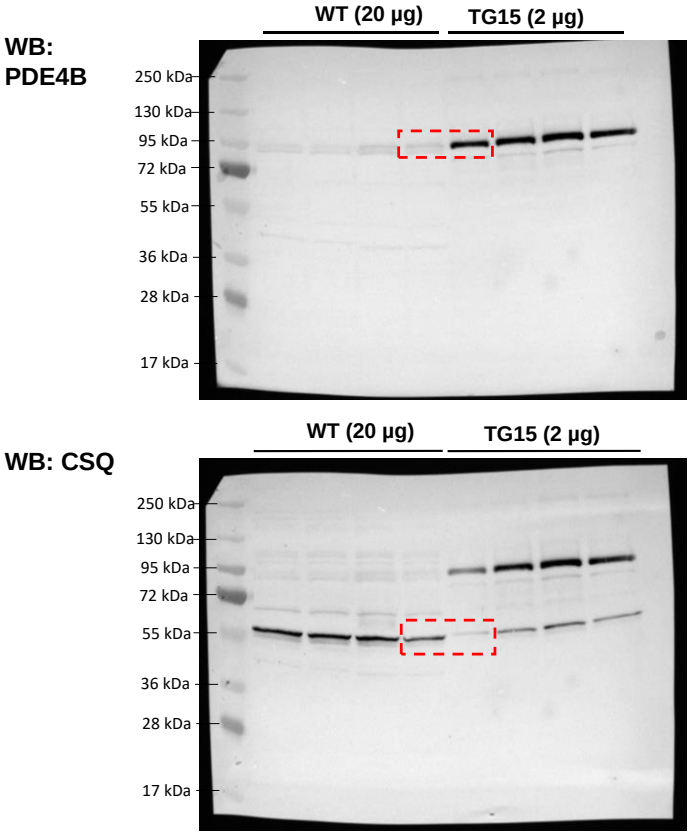

Figure 2H

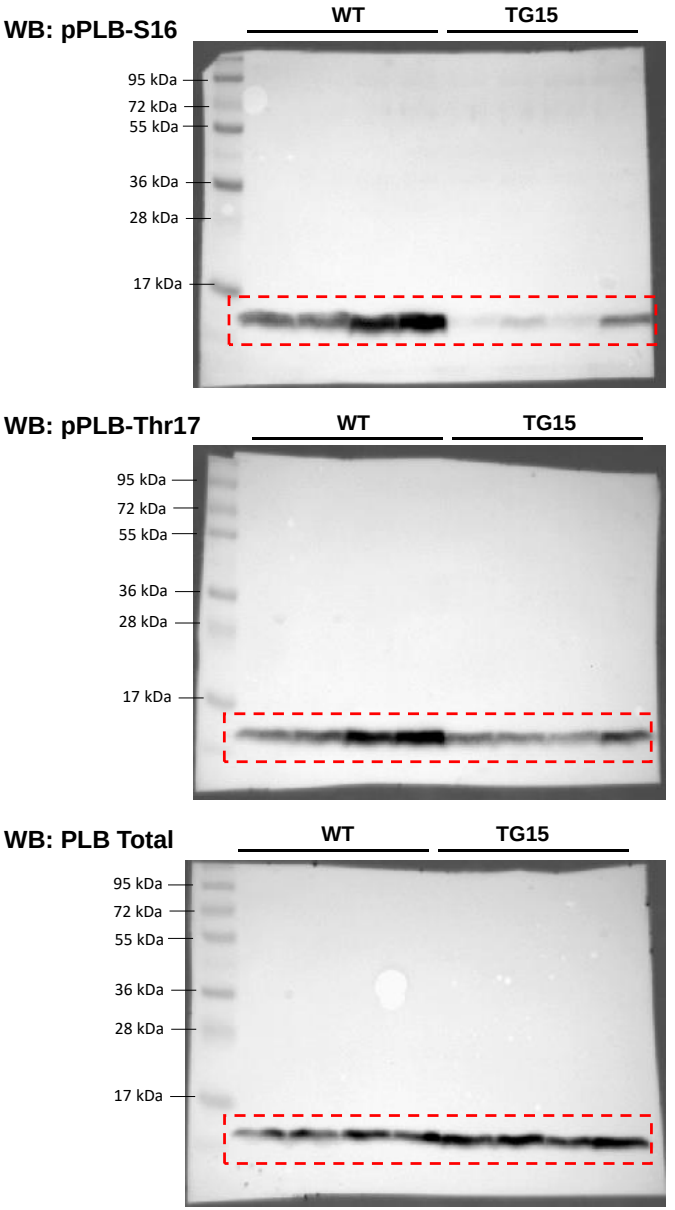

Figure 2I

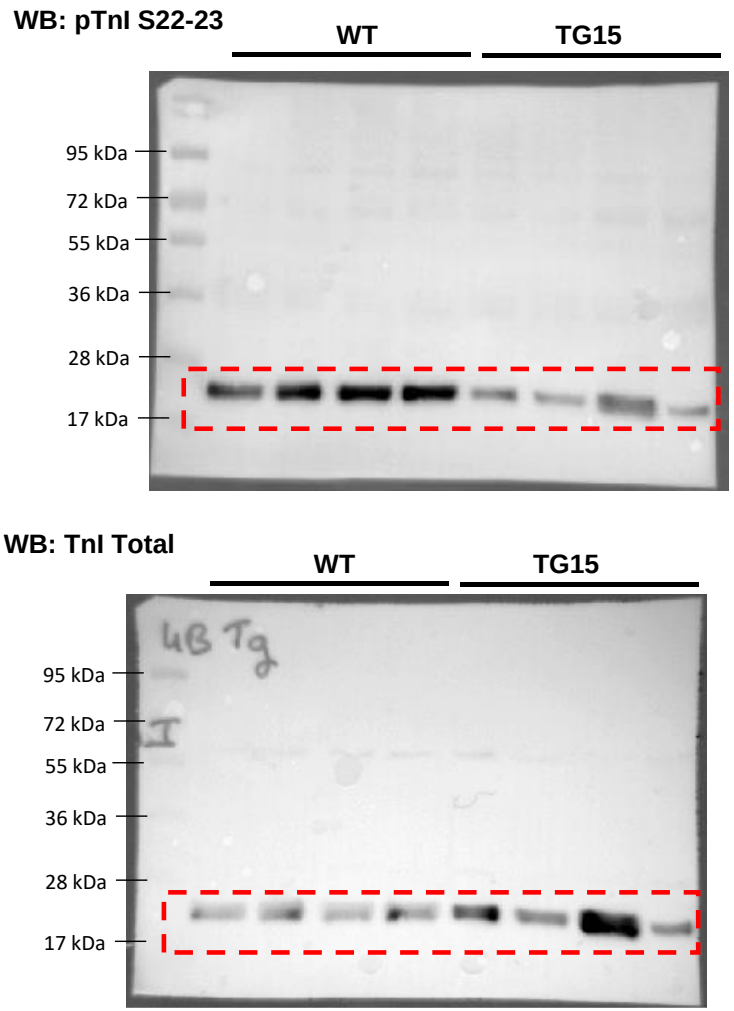

Figure 2J

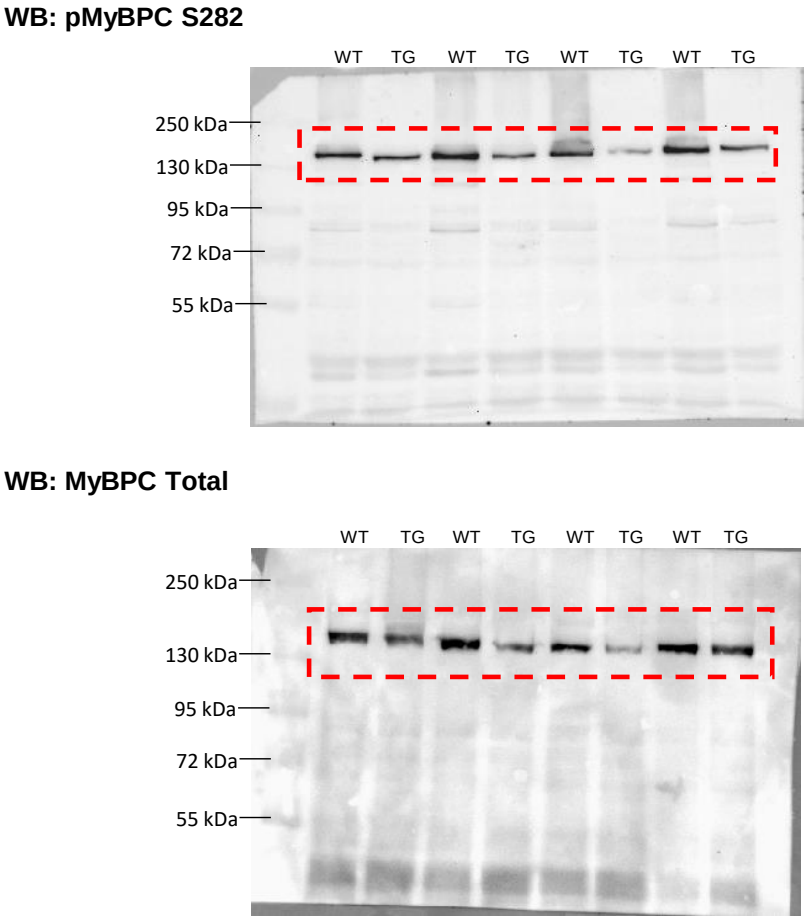

Supplemental Figure 1A

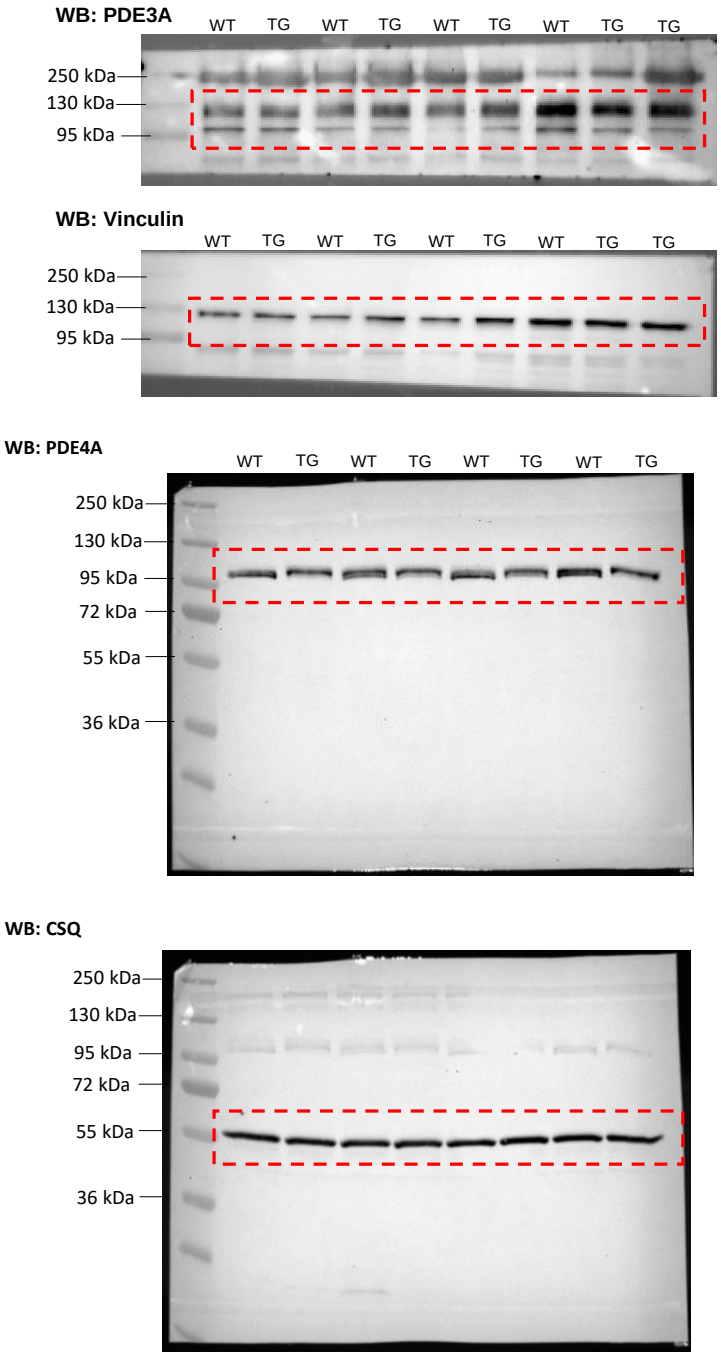

Supplemental Figure 3C

WB: PDE4B

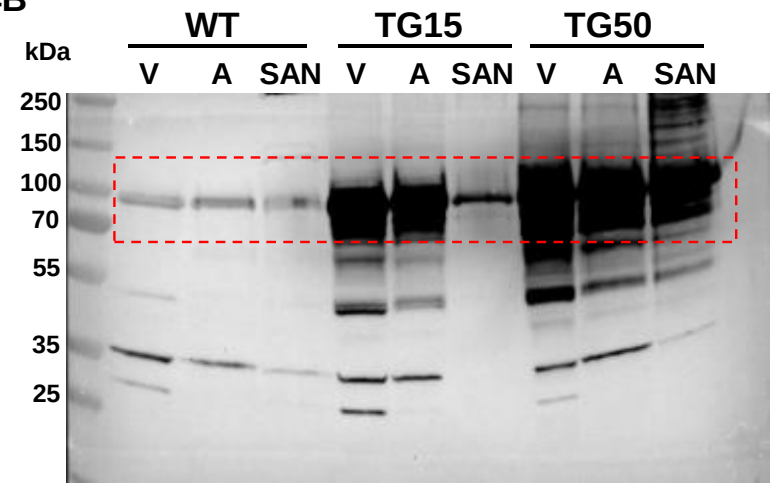

WB: calsequestrin

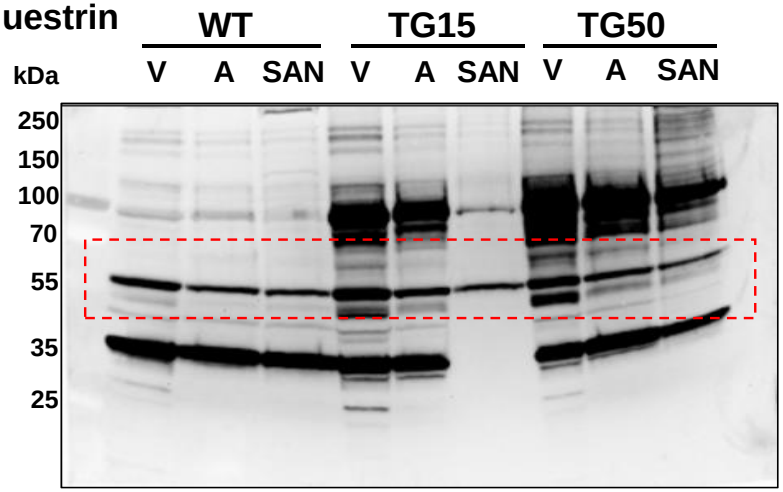

Supplemental Figure 5

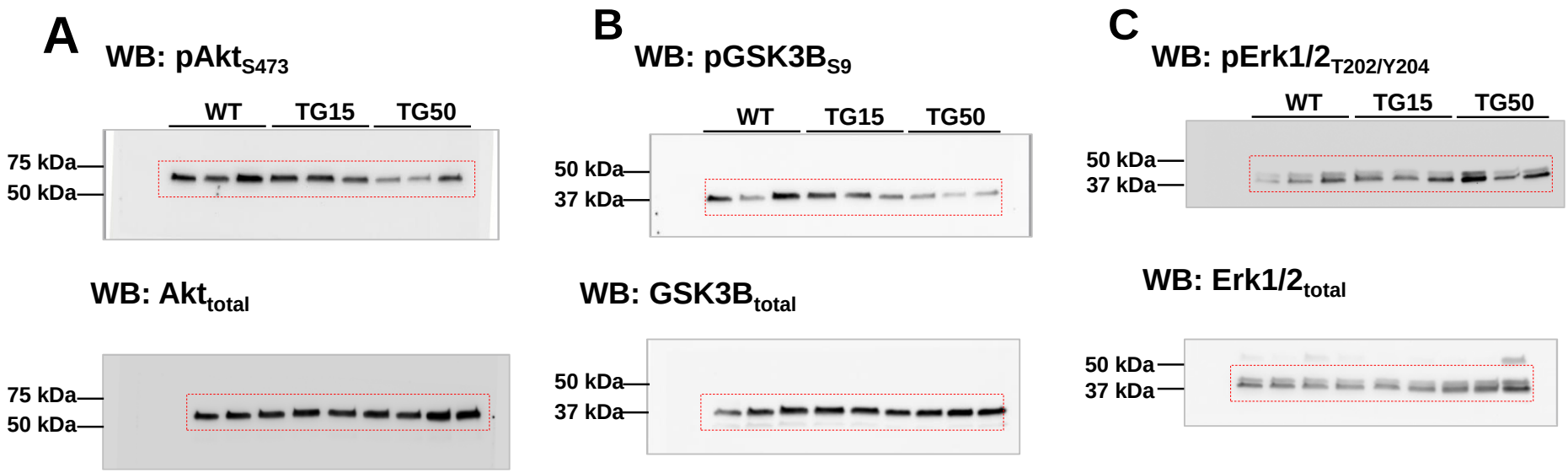

Supplemental Figure 10B

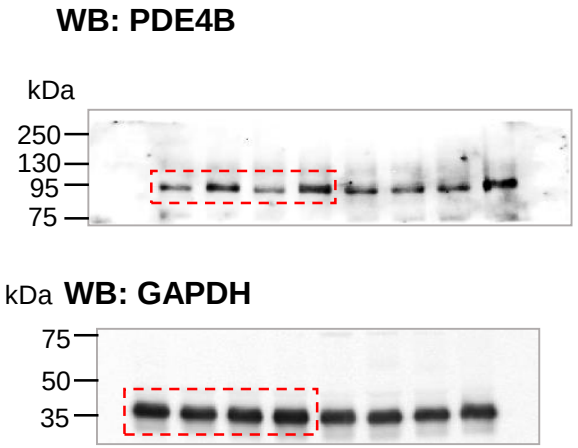

Supplemental Figure 11B

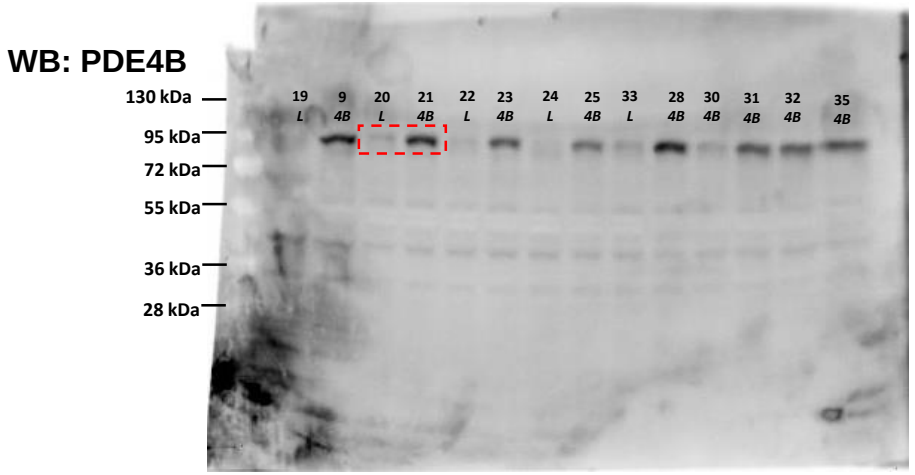

Supplemental Figure 11A